

CONFERENCES AND SYMPOSIA

PACS numbers: 95.55.Ka, **96.60.–j**, 96.60.Q–, 96.60.qe

Microflares and nanoflares in the solar corona

S A Bogachev, A S Ulyanov, A S Kirichenko, I P Loboda, A A Reva

DOI: https://doi.org/10.3367/UFNe.2019.06.038769

Contents

Abstract. Due to the increase in the spatial and temporal resolution of observations of the solar atmosphere, which is mainly associated with progress in space research, we now understand that the Sun's activity not only is associated with large centers, but also extends to significantly smaller scales. Each new advance in experimental technology over the past 60 years has led to the discovery of more and more numerous and small solar structures: X-ray active regions in the 1960s, hot X-ray points in the 1970s, solar microflares in the 1980s, and finally, from the end of the 20th century, solar nanoflares. At the same time, the total energy release, obtainable from observations, is still insufficient to ensure a balance between heating of the corona and its rapid radiative cooling. For the smallest-scale phenomena, nanoflares, it is still not possible to resolve their structure and mechanism, which raises the question of whether it is correct to classify them as flares. We present a review of the main results obtained so far in the field of small-scale solar activity, mainly microflares and nanoflares, and discuss the main issues that need to be solved in order to move forward.

Keywords: solar corona, solar activity, solar microflares, solar nanoflares, hot X-ray points, Ellerman bombs

1. Introduction

It is believed that the term nanoflare as applied to solar physics was introduced in 1988 by E Parker [1], an outstanding American astrophysicist whose brilliant scientific achievements also include the prediction of solar wind 'with the point of his pen' in the late 1950s [2]. Parker hypothesized the existence of nanoflares, besides normal-sized flares, in the solar corona, releasing $10^{-9}-10^{-6}$ times the energy of their ordinary analogs. Parker arrived at this conclusion after careful consideration of the mechanism maintaining high coronal temperature. At a temperature of $(1-2)\times 10^6$ K, the corona loses heat through extreme ultraviolet (UV) and X-ray radiation at a rate of $10^5-5\times 10^6$ erg cm^{-2} s^{-1} (see, e.g., [3]), which raises a question about the mode of replenishment of this energy.

The prevailing opinion at Parker's time (still advocated by many nowadays) was as follows. Convective plasma movements in the upper layers of the Sun generate acoustic and magnetohydrodynamic waves propagating into higher layers of the solar atmosphere, where they dissipate and heat the surrounding gas. Schwarzschild [4] was among the first to express this idea in 1948. However, a more detailed analysis shows that waves of all types, except Alfven waves, dissipate or reflect before they reach the corona (see, e.g., the comprehensive review by Stein and Leibacher [5], as well as [6, Ch. 4]).

In other words, the Alfven waves in a plasma are the sole carrier capable of convective motion energy transfer from the Sun's surface to the corona. But the ability of Alfven waves to propagate over long distances without dissipation creates another problem, i.e., how to make them dissipate energy and heat the corona. Ideas have been proposed on (see, e.g., [7, 8]) based on the relationship between Alfven waves of different scales and their resonant absorption in certain coronal layers. However, such an approach, as a rule, implies a large amplitude of Alfven waves, in conflict with observations, because high-amplitude waves must be readily identifiable in experiments designed to study oscillations of small-scale magnetic structures in the Sun's atmosphere (e.g., observations of spicules).

Advances in experimental technology over the past 20 years have markedly improved the angular resolution of observed phenomena and given rise to numerous publications concerning the experimental registration of magnetic structure oscillations in the solar corona, such as [9] (the first

S A Bogachev [1,2,a], **A S Ulyanov** [1,b], **A S Kirichenko** [1,c], **I P Loboda** [1,d], **A A Reva** [1,e]
[1] Lebedev Physical Institute, Russian Academy of Sciences, Leninskii prosp. 53, 119991 Moscow, Russian Federation
[2] Samara National Research University, ul. Moskovskoe shosse 34, 443086 Samara, Russian Federation
E-mail: [a] bogachev@lebedev.ru, [b] ulyanovas@lebedev.ru, [c] kirichenkoas@lebedev.ru, [d] lobodaip@lebedev.ru, [e] revaaa@lebedev.ru

Received 5 June 2019
Uspekhi Fizicheskikh Nauk **190** (8) 838 – 858 (2020)
Translated by Yu V Morozov; edited by V L Derbov

report of results obtained by the Transition Region And Coronal Explorer (TRACE)), [10] (data from the Space Optical Telescope (SOT) aboard the Hinode satellite), [11] (data taken by the Atmospheric Imaging Assembly (AIA) mounted on the Solar Dynamics Observatory (SDO)), and even experimental observations of resonant wave absorption in the solar corona [12]. For all that, the role of propagation and dissipation of Alfven waves in the mechanism of coronal heating is still not confirmed by observations. Possibly, progress on this issue will be achieved by direct measurement of solar plasma characteristics near the Sun, expected to be made over the course of the Parker Solar Probe mission. The first results suggest the presence of high-amplitude Alfven waves in the solar wind plasma [13]. However, measurements in orbits closer to the Sun are needed not only to confirm the presence of Alfven waves but also to draw more convincing conclusions as regards their propagation and dissipation and thereby either verify or refute the respective coronal heat models.

The alternative proposed by Parker based on his earlier theoretical assumptions (see [14]) consisted of the assumption that the energy transfer from the Sun's convective layer into the corona is possible by dissipation of both waves and electric currents. The interaction of oppositely directed magnetic fluxes in the rarified coronal plasma characterized by high electric conductivity is known to give rise to current layers distributed over the surface separating the fluxes and preventing the interpenetration (reconnection) of magnetic fields [15, 16]. As far as small-scale magnetic fields of the solar corona are concerned, their bases resting on the Sun's surface must be continuously displaced by surface convective flows of the plasma, which causes a braiding of magnetic lines, the formation of numerous small-scale current layers, and, accordingly, the accumulation of magnetic energy. A balance between Joule heating and radiative cooling in the current layers is possible for a certain time. After the balance becomes impossible, a nonstationary explosive phase of current layer decay begins with the release of the accumulated energy, interpreted as the pulsed phase of a solar flare. If this mechanism operates in small-scale current layers of the lower corona, the process of their dissipation can be explosive too and manifested as flares with much lower energy, i.e., nanoflares.

One of the most important experimental proofs of the validity of this assumption available at that time (the late 1980s) was provided by observations of solar hard X-ray radiation in which a fine structure was discovered owing to high temporal resolution of the detection method. Specifically, Lin et al. [17] used balloon-borne instrumentation (June 27, 1980) and recorded approximately 25 solar bursts with a photon energy of ~ 20 keV, which lasted from a few seconds to several tens of seconds and had nonthermal power-law energy spectra ($I \sim E^{-\gamma}$). Nonthermal solar radiation in the X-ray wavelength range largely arises in the chromosphere when solar flare-accelerated electrons slow down. Based on this assumption (the so-called thick target model [18, 19]), the authors of [17] calculated the energy of electrons needed to generate bursts with the observed spectrum and intensity and showed that they are individual events (flares) with an energy of $10^{26} - 10^{28}$ ergs. This energy is roughly 10^{-6} of the large flare energy. Therefore, such events should be referred to as microflares. However, Parker noticed that the observed radiation profiles (Fig. 1) consist of many smaller bursts with an energy of approximately 10^{24} ergs, which can be interpreted as multiple frequent bursts; he proposed that they be called nanoflares. True, it was admitted that instrumental constraints preclude observations needed to make more reliable conclusions.

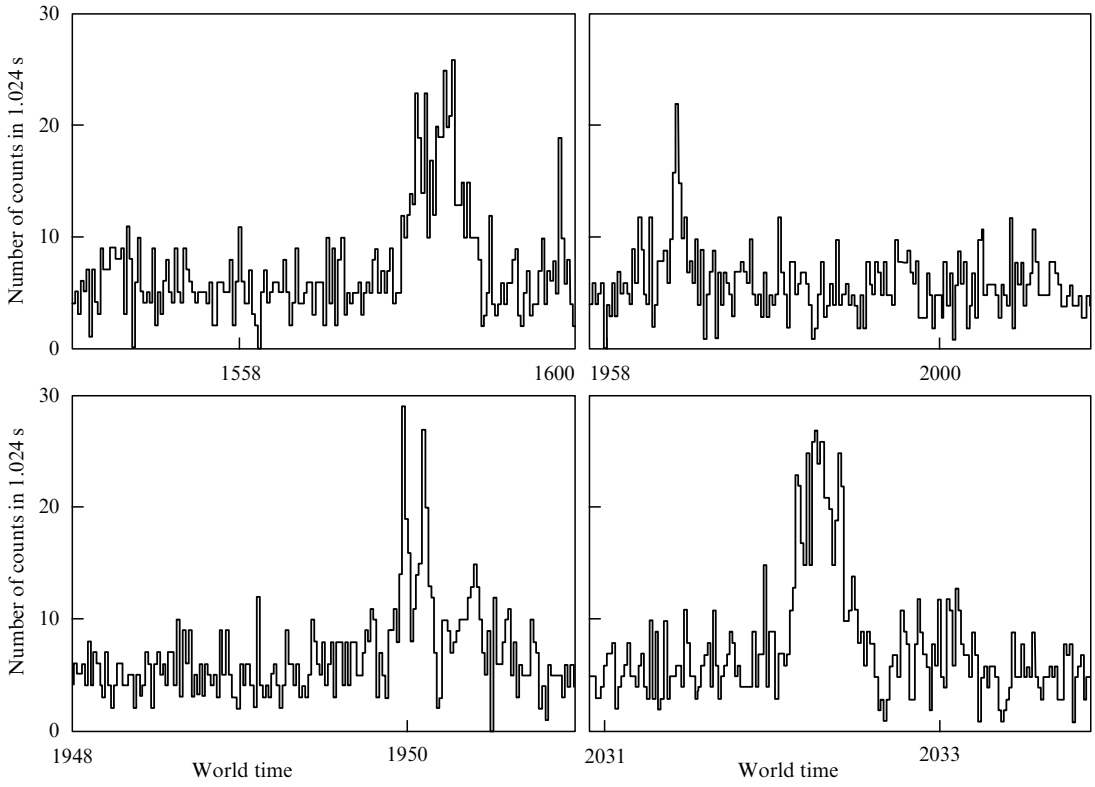

Figure 1. Radiation profiles of solar X-ray microflares obtained in the 22–33 keV range with a temporal resolution of 1.024 s (based the data from [17]).

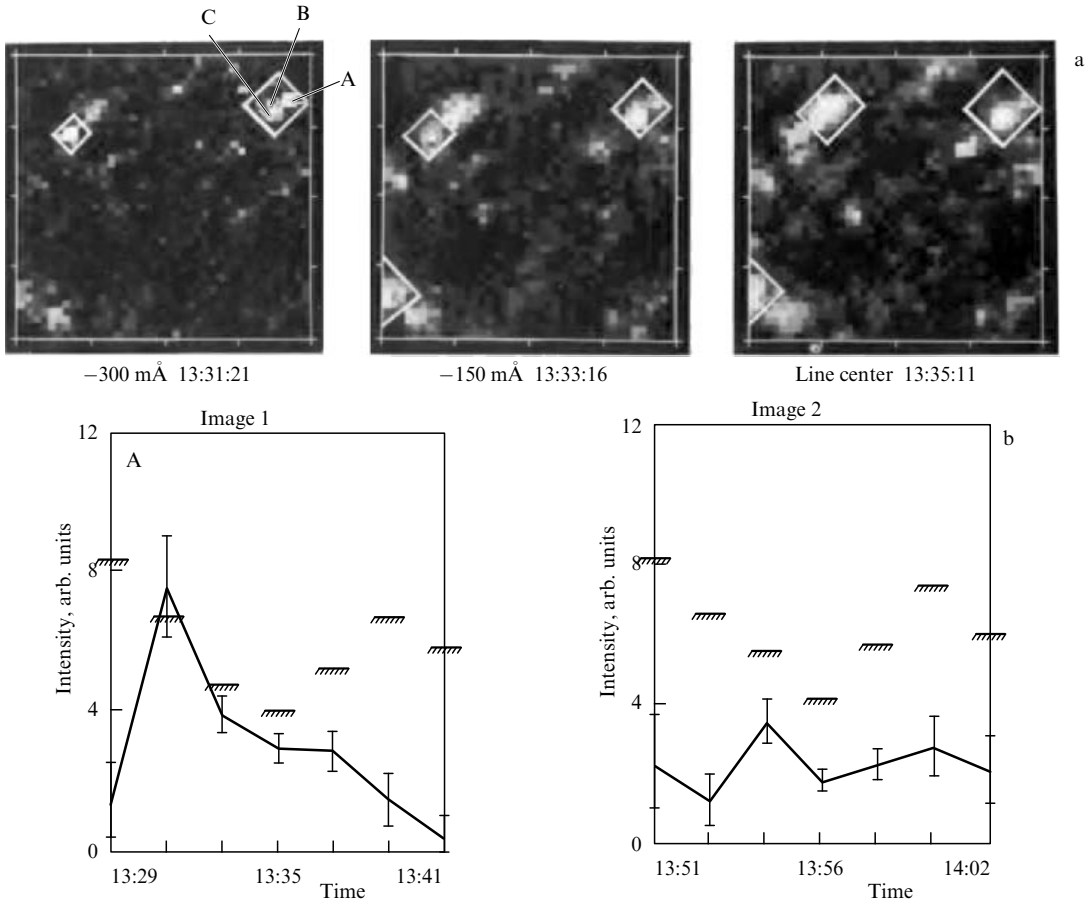

Figure 2. Telescopic observations of small-scale emission cores in the solar corona during the SMM space mission [20]: (a) three successive images of one section of the Sun on the C_{IV} 1548-Å line, (b) temporal radiation profile in emission core A (normalized to mean image intensity) — the shortest of the bursts recorded so far.

The Solar Maximum Mission (SMM) spacecraft operating in orbit from 1980 to 1989 provided images of small-scale emission structures localized in the Sun's upper chromosphere [20] that were interpreted as UV analogs of previously observed fast X-ray bursts (Fig. 2). The images displayed the emitting structures in the C_{IV} 1548-Å spectral line and were spatially localized in quiet areas of the Sun's atmosphere, lacking large-scale activity. A comparison with magnetic field maps and simultaneously taken images of the chromosphere demonstrated that cores were formed in the vicinity of small-scale dipole magnetic structures and located largely near chromospheric network boundaries, i.e., in proximity to granular cell boundaries. This pattern fits with the physics of solar flares resulting from interaction between magnetic fluxes of opposite polarity; it agrees with the key role of convective processes in the formation of minor flares.

Taken together, evidence available by the end of the 1980s suggested that solar activity is not associated with large structures (e.g., sunspots) alone but just as well manifests itself at a much smaller scale. Moreover, it became obvious that each noticeable advance in the accuracy of experimental studies revealed more and more numerous small-scale structures, such as X-ray active regions and flares in the 1960s [21–24], X-ray bright points in the 1970s [25, 26], and microflares in the 1980s [17, 20, 27]. Taking account of this tendency, it was only natural to suggest that such series can be hypothetically extended to structures and events on an even smaller scale; as a result, the term nanoflare was coined.

This publication is an attempt to overview current studies on small-scale solar activity with special reference to micro- and nanoflares. We do not mean, however, that the modern classification is restricted to these two classes but only define the framework of the article. We present the main results obtained so far in the field of small-scale solar activity and discuss the fundamental issues that need to be solved in order to move forward.

2. Energy distribution of microflares and nanoflares

The theory of formation of the hot solar corona developed by Parker attracted the attention of researchers to low-energy flares. The energy distribution of the flares plays the key role in the heating of the corona. To demonstrate this, it should be mentioned in the first instance that the total amount of coronal thermal energy is relatively small; it is comparable to the energy released in a large solar flare. To estimate it, we suggest that the corona is in hydrostatic equilibrium:

$$k_B T \frac{dn}{n} = -m g_0 \frac{R_0^2}{r^2} dr,$$

where R_0 is the solar radius, m is the mean particle mass ($0.6 m_p$ for the corona), g_0 is the free fall acceleration at $r = R_0$, k_B is the Boltzmann constant, and T is the coronal temperature, regarded for simplicity as a height-independent

variable. In this case,

$$n(r) = n_0 \exp\left[\frac{R_0^2}{H_0}\left(\frac{1}{r} - \frac{1}{R_0}\right)\right],$$

where $H_0 = mg_0/(k_B T) \approx 5 \times 10^4$ km. Then, the following number of particles,

$$N = \int_{R_0}^{2R_0} n(r) 4\pi r^2 \, dr = 4\pi n_0 \exp\left(-\frac{R_0}{H_0}\right) \times \int_{R_0}^{2R_0} \exp\left(\frac{R_0^2}{H_0 r}\right) r^2 \, dr,$$

is contained in a height range from one to two solar radii, where most of the coronal mass is concentrated; it yields

$$N \approx 4.5 \times 10^{41}.$$

The total thermal energy of the solar corona is

$$E_{\text{therm}} = \frac{3}{2} N k_B T \approx 10^{32} \text{ erg}. \quad (1)$$

In other words, the thermal energy of the corona can be fully replenished by solar flares in which an energy of $10^{30} - 10^{33}$ erg or more is released; moreover, plasma heating from several MK to 10–30 MK and even 100 MK (so-called superhot plasma) is observed in experiment. However, the main problem is stable maintenance of the high temperature over the solar cycle rather than hot plasma formation. Indeed, natural heat emission from the quiet solar corona, which at 1 MK occurs largely in the EUV spectral region, must result in its radiative cooling at the rate about $F = 10^5$ erg cm^{-2} s^{-1} inherent in the quiet corona (see, e.g., [3]). A comparison of this value with (1) gives the characteristic cooling time of the solar corona

$$\tau = \frac{E_{\text{therm}}}{4\pi R_0^2 F} \approx 4 \text{ h}. \quad (2)$$

The overall energy loss in the corona per unit time

$$F_{\text{therm}} = 4\pi R_0^2 F \approx 6 \times 10^{27} \text{ erg s}^{-1}. \quad (3)$$

It is easy to show that large solar flares occur too rarely to make up for this loss. According to the National Oceanic and Atmospheric Administration (NOAA) catalog of solar flares, 7755 X-ray flares of C class giving rise to a flux of soft X-ray radiation in the wavelength range from 1 to 8 Å at Earth's orbit level were recorded in the solar disk during the past 24th solar cycle (2009–2019, inclusive) together with 740 M class flares (a flux from 10^{-5} to 10^{-4} W m^{-2}) and 49 X class flares (a flux over 10^{-4} W m^{-2}). An assumption that the largest X, M, and C class flares have a total energy of $\sim 10^{32}$, $\sim 10^{31}$, and $\sim 10^{30}$ erg, respectively, and that a similar number of flares occurred during this time on the far side of the Sun, leads to the conclusion that the total energy of the large-scale outburst activity during the 24th solar cycle was $\sim 4 \times 10^{34}$ erg. To recall (for correct evaluation of the role of flares in the solar energy balance), the sun emits such energy in the optical radiation wavelength range for only 10 s. Dividing this value by the cycle length yields for flares

$$F_{\text{fl}} \approx 8 \times 10^{25} \text{ erg s}^{-1}. \quad (4)$$

A comparison of (3) and (4) gives an energy deficit of ordinary flares relative to radiative losses of around 99% averaged over a solar cycle. Moreover, the frequency of flares is considerably reduced during solar minima (large flares may not be observed at all for 2–3 years), which makes the energy deficit even more pronounced. For example, a calculation analogous to (4) for the 2019 minimum between the 24th and 25th cycles gives $F_{\text{fl}} \approx 2 \times 10^{24}$ erg s^{-1}. Nonetheless, the corona remains hot and retains its usual thermal energy budget.

It follows from the foregoing that the frequency of flares is a key parameter in the flare heating theory. Large flares being incapable of proper heating, the missing energy can be contained in small-scale flares provided that they are sufficiently frequent. Indeed, if the frequency of flares with an energy of 1/10 that of C class flares is 10 times higher or more than the frequency of the C class flares, while their integral energy release is greater than in the C class flares, despite a lower energy of each individual event. Otherwise, they would release less energy and are of no use for the solution to the energy shortage problem.

More accurate calculations of this kind were undertaken in 1991 by Hudson [28], who collected results of observations of flaring activity in the hard X-ray wavelength range and evaluated the total power released by flares and microflares in the solar corona. Hudson estimated it to be 2×10^{25} erg s^{-1} or 2–3 orders of magnitude lower than the total coronal radiation power in the X-ray range (see [29] in addition to the aforementioned references). Hudson plotted a frequency distribution of events depending on their energy from 10^{27} to 10^{33} erg (Fig. 3), showed that it is fairly well described by the power-law dependence $N(E) = AE^{-\alpha}$ with $\alpha \approx 1.8$, and then extrapolated it to the low-energy region.

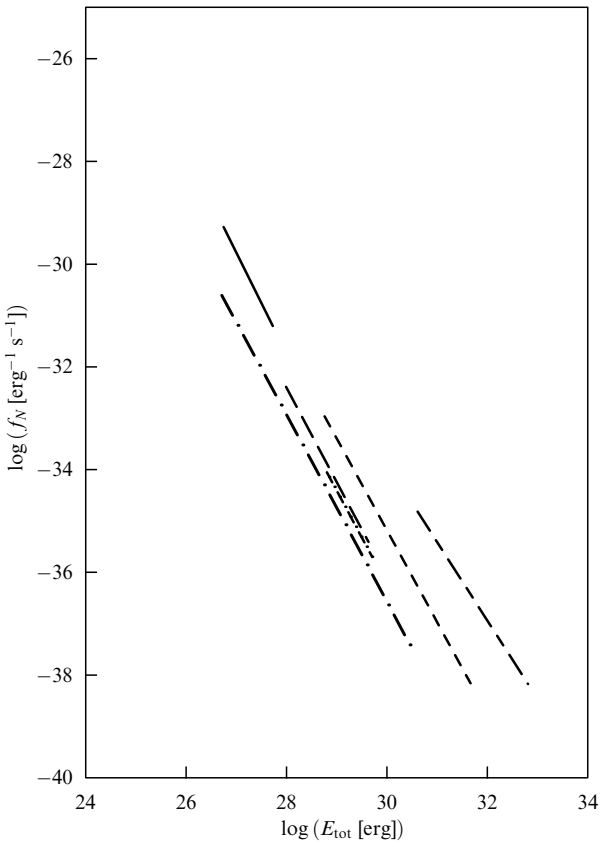

Figure 3. The dependence of solar flare frequency f_N on the total flare energy E_{tot} in an energy range of $10^{27} - 10^{33}$ erg derived by Hudson [28] from the results of various X-ray observations of the Sun in 1971–1989.

For the power-law distribution of flares with exponent α, the total flare energy in a range from a certain minimal value E_0 to a maximum one E_1 is given at $\alpha \neq 2$ by the integral

$$P = \int_{E_0}^{E_1} AE^{-\alpha} E\,\mathrm{d}E = \frac{A}{2-\alpha}\left(E_1^{2-\alpha} - E_0^{2-\alpha}\right). \quad (5)$$

Let us consider a range limited by an order of magnitude energy, say, from 10^{29} to 10^{30} erg, i.e., assume that $E_1 = 10E_0$. In this case, Eqn (5) takes the form

$$P_{10} = AE_0^{2-\alpha}\,\frac{10^{2-\alpha}-1}{2-\alpha}. \quad (6)$$

Differentiation of (6) with respect to E_0 yields

$$\frac{\mathrm{d}P_{10}}{\mathrm{d}E_0} = (2-\alpha)\,\frac{P_{10}}{E_0}. \quad (7)$$

It means that a reduction in E_0 at $\alpha > 2$, i.e., a transition from ordinary flares to micro- and nanoflares, raises the integral energy in events of new classes; conversely, the energy decreases if $\alpha < 2$. The case of $\alpha = 2$ corresponds to the uniform energy distribution among flares of all classes.

The value of α derived by Hudson from Fig. 3 was 1.8 (see above). In other words, the only way to correlate the hypothesis of flare-driven coronal heating with observations is to assume that the distribution of flares with energies below 10^{27} erg (nanoflares) must differ from that of ordinary flares and microflares with power-law index $\alpha > 2$, which implies that they have different physical nature. Testing this hypothesis was the principal objective of observations of low-energy flares in the soft X-ray (SXR) and extreme ultraviolet (EUV) wavelength ranges.

The observation of microflares in the SXR range in the quiet solar corona was reported for the first time by Krucker et al. [30] in 1997 (i.e., six years after Hudson's publication) based on the data obtained by the Soft X-ray Telescope (SXT) on board the spaceborne Yohkoh solar observatory [31]. A distinctive feature of the observed events was an insignificant rise in temperature, at first sight in conflict with a noticeable burst of radiation. The authors hypothesized that radiation enhancement was in the first place due to an increased emission measure (emitting plasma volume and density), while the bursts themselves were caused by plasma evaporation from the chromosphere into the corona, similar to the formation of SXR radiation in large solar flares.

The most known observations in the EUV range are those reported by Berghmans et al. [32] in 1998, who discovered a large number of 10–12-min-long transient brightenings and identified the new events as nanoflares based on the data obtained by the Extreme-Ultraviolet Imaging Telescope (EIT) [33] aboard the Solar and Heliospheric Observatory (SOHO).

Krucker and Benz [34] suggested that EUV brightenings observed by Berghmans et al. are of the same nature as SXR radiation bursts in microflares. Plasma evaporation from the chromosphere into the corona must change EUV-radiation intensity as follows:

$$\Delta I = \left(\frac{\Delta N_\mathrm{e}}{V}\right)^2 R(T)V = \frac{(\Delta N_\mathrm{e})^2 R(T)}{V}, \quad (8)$$

where ΔN_e is the number of electrons injected into the volume V, T is the plasma temperature, and $R(T)$ is the temperature response function of the telescope. If variation of thermal energy E_therm is used to estimate energy release during a flare, then

$$E_\mathrm{therm} = 3\Delta N_\mathrm{e} k_\mathrm{B} T = 3k_\mathrm{B} T\sqrt{\frac{V\Delta I}{R(T)}}. \quad (9)$$

The unknown variables in Eqn (9) are temperature T and volume V. To measure the temperature, Aschwanden et al. [35] proposed the filter ratio method, based on the recording of the same event in at least two independent observation channels with known temperature response functions and determining the temperature based on the ratio of signals from the channels. The authors of [35] used the data from the 171-Å and 195-Å channels (observation wavelengths corresponding to the spectral lines of highly ionized iron) of the TRACE telescope [36]. If plasma temperature is assumed to be equal over the entire volume at each point in time (a single-temperature approximation), with the temperature response functions of the channels being known, the ratio of intensities in the channels from Eqn (8) must be equal to the ratio of responses:

$$\frac{\Delta I_{171}}{\Delta I_{195}} = \frac{R_{171}(T)}{R_{195}(T)} \equiv q(T). \quad (10)$$

This means that temperature T can be calculated from the ratio of intensities in accordance with the known dependence $q(T)$.

It is also possible to estimate the temperature of micro- and nanoflares from model dependences on other plasma parameters. The best known example of such dependence is the Rosner–Tucker–Vaiana (RTV) scaling law [37], fairly well satisfied for quiet Sun regions:

$$T \sim (pL)^a, \quad (11)$$

where T and p are the plasma temperature and pressure, and L is the length of the coronal loop. The exponent a obtained by Rosner is 1/3, but Aschwanden showed in [38] that, in the case of flare heating, this value can be somewhat lower ($a \approx 1/4$) due to nonstationary heating.

The estimation of volume V in calculations of the energy of small flares using (9) encounters difficulty because the geometry of the radiation source appears unknown due to the projection effect. In such a case, it is assumed that the emitting region is a coronal loop having a constant cross section over its entire length, and the volume is calculated using the equation

$$V = \frac{\pi d}{2}\,\frac{\pi w^2}{4} = \frac{\pi^2 d w^2}{8}. \quad (12)$$

The loop diameter d in (12) is determined from the observed size of the emitting region, while cross section w is found by modeling. In the simplest case, w is assumed to be constant. In more complicated models, the size of coronal loops obeys the similarity principle, which allows the cross section to be found from the diameter d.

Since the characteristic size of a radiation source in micro- and nanoflares amounts to thousands of kilometers, the accuracy of the energy estimation strongly depends on the spatial resolution of the measuring instruments. For this reason, weak flares are, as a rule, observed using high-

Table 1. Main research studies on nanoflare energy distribution.

References	Device (channel, Å)	Number of events	Energy range, erg	Exponent α
Berghmans at al. [32] (1998)	EIT (304, 195)	9187	$10^{24}-10^{27}$	1.9, 1.35
Aschwanden et al. [35] (2000)	TRACE (171, 195)	281	$10^{24}-10^{26}$	1.79
Parnell, Japp [41] (2000)	TRACE (171, 195)	4497	$10^{23}-10^{26}$	2.4
Benz, Krucker [42] (2002)	EIT (171, 195)	11,150	$10^{25}-10^{27}$	2.3
Aschwanden, Parnell [43] (2002)	TRACE (171, 195)	436, 380	$10^{25}-10^{27}$	1.86, 1.81
Ulyanov et al. [40] (2019)	TESIS, AIA (171)	107,075	$10^{23}-10^{26}$	2.2–2.9

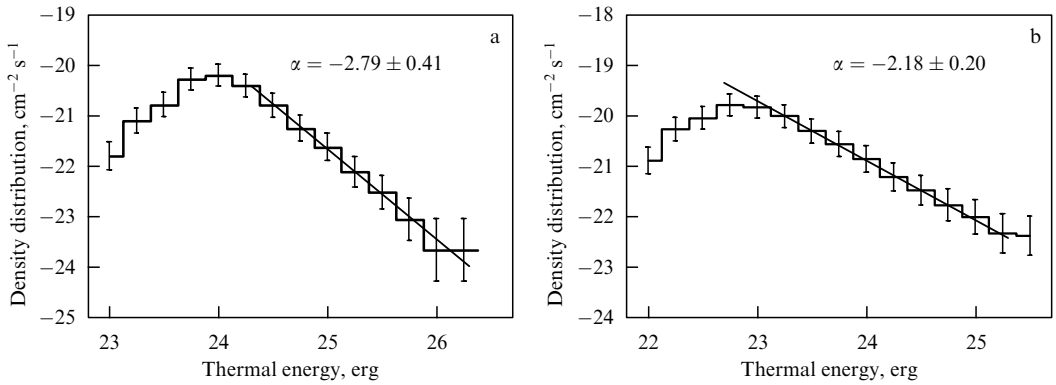

Figure 4. Nanoflare energy distribution (on logarithmic scales) obtained in [40] based on the results of TESIS/CORONAS-Photon (a) and SDO/AIA (b) observations.

resolution telescopes and spectrographs. Recent progress in this field has been achieved with the use of the AIA four-telescope array aboard SDO and the High Resolution Coronal Imager (Hi-C) telescope. The time resolution of the telescope is equally important in light of the transience of observed dynamics. At present, the highest temporal resolving power is shown by the TESIS telescope-spectroheliograph assembly (solar telescope/imaging spectrometer) operated aboard the CORONAS-Photon satellite (Complex Orbital Observations Near-Earth of Activity of the Sun-Photon) [39]. The shortest time interval between images recorded in one channel was 4 s.

The summary on the main results of the statistical analysis of the weak flare energy distribution is presented in Table 1. Clearly, the currently available data are not yet sufficient to say confidently that the distribution of small flares actually obeys the $\alpha > 2$ law. The recent data obtained by Ulyanov and co-workers [40], who compared the results of TESIS and AIA observations during a minimum of solar activity and during its rising phase, show that the index of the power-law nanoflare energy distribution falls into the range $\alpha = 2.2-2.9$, thus giving evidence in favor of the nanoflare heating theory (Fig. 4). At the cycle minimum, the α value was higher than in its rising phase, which suggests an energy-dependent redistribution of the flare frequency during the cycle. All the same, the integral energy release from the recorded events proved to be approximately 30 times smaller than is needed to maintain a balance between energy loss and gain in the corona, meaning that the resolving power of measuring devices must be further improved if the cause of corona heating is to be elucidated.

3. High-temperature plasma in low-energy flares

Continuous solar flare radiation mainly occurs in the short wavelength region of the spectrum. It consists of a non-thermal component showing a power-law energy distribution and thermal radiation having the Maxwellian spectrum. The thermal radiation is registered at energies up to 10–30 keV (see [44]), which corresponds to the solar flare plasma temperature up to $(10-30) \times 10^6$ K, although a plasma with $T \sim 100 \times 10^6$ K (so-called superhot plasma) is sometimes observed [45]. Note that such temperatures are an order of magnitude higher than in the solar core. In the spectral region above 50 keV, all continuous solar radiation has a non-thermal origin; in other words, it forms by virtue of high-energy particle deceleration in dense plasma.

For small-scale solar flares, the possibility of differentiating radiation into thermal and nonthermal components is less obvious. The number of currently available observations of nonthermal radiation in microflares (see, for instance, [46, 47]) is rather small; the thermal component alone is registered in the majority of events, while the nonthermal component in nanoflares remains to be discovered. Moreover, there is no consensus on the identity of mechanisms underlying nanoflares and usual flares. Also, it is equally unclear whether it is correct to extrapolate the patterns of large-scale events to nanoflares.

The question concerning the temperature to which plasma can be heated during micro- and nanoflares is directly relevant to the problem of coronal heating. Evidently, the formation of a high-temperature corona is impossible if the total energy of small-scale flares, no matter how high, is released only in the low-temperature region. Because a reduction in the flare power results in a drop in flare plasma temperature, as inherent in ordinary flares, there must be a certain threshold flare power below which the flare contribution to coronal heating becomes insignificant.

The flare power is traditionally characterized in terms of the Geostationary Operational Environmental Satellite (GOES) classification based on the measurement of SXR radiation fluxes in a 1–8-Å range in Earth's orbit. The GOES

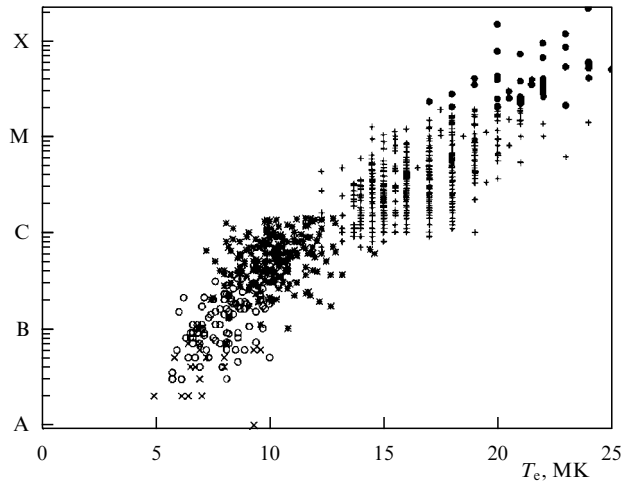

Figure 5. Dependence of the flare X-ray class on plasma electron temperature T_e measured by GOES sensors at the maximum radiation level in the 1–8-Å range (from Feldman et al. [48]).

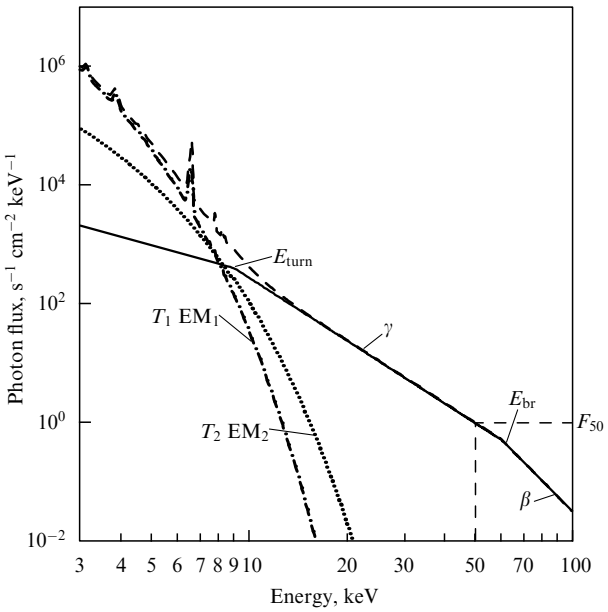

Figure 6. Model approximation of RHESSI experiment spectra (dashed curve) by two thermal components with temperatures T_1 (dashed-dotted curve) and T_2 (dotted curve) and non-thermal component with slope γ in an energy range below 50 keV and with slope β in an energy range above 50 keV. EM_1 and EM_2 are emission measures (from [51]).

flare scale falls into the classes A, B, C, M, and X, corresponding to radiation fluxes from 10^{-8} to 10^{-7} W m^{-2} (A class), from 10^{-7} to 10^{-6} W m^{-2} (B class), from 10^{-6} to 10^{-5} W m^{-2} (C class), from 10^{-5} to 10^{-4} W m^{-2} (M class), and from 10^{-4} W m^{-2} (X class), respectively. A digital postfix (the multiplier factor) is added to each literal notation; for example, the M2.4 class notation indicates that a radiation flux of 2.4×10^{-5} W m^{-2} was registered in the 1–8-Å range during a flare maximum at Earth's orbit level. To recall, the GOES scale, designed to classify ordinary flares, lacks levels corresponding to nanoflares. The minimal A class roughly corresponds to the largest microflares with energies equal to 10^{28} erg or so.

Feldman et al. [48] were among the first to elucidate the relationship among electron temperature of the flaring plasma, its X-ray flare class, and emission measure. They analyzed a sample of 868 flares of A2 to X2 classes based on the data obtained with the use of the Bragg Crystal Spectrometer (BCS) aboard the Yohkoh observatory [49] and GOES X-ray monitor [50]. The temperature was deduced from BCS spectra measured near three resonance helium-like lines: Fe XXV ($\lambda = 1.85$ Å), Ca XIX ($\lambda = 3.18$ Å), and SXV ($\lambda = 5.04$ Å). The T value was selected based on the condition of maximum correlation between the observed and theoretical spectra. The resulting relationship between the X-ray flux of the flare F and flaring plasma temperature T had an exponential shape (Fig. 5).

Battaglia at al. [51] undertook a detailed analysis of 85 flares of B1 to M6 classes after background subtraction based on the data of the Ramaty High Energy Solar Spectroscopic Imager (RHESSI) [52]. Plasma parameters were determined for the maximum of hard X-ray radiation from the flares, unlike the parameters in Feldman's study, where the peak in the low-energy spectral region that usually appears later was considered. To determine plasma temperature, the shape of the flares' continuous radiation spectra was analyzed following their approximation with the use of the SPEX software package [53, 54]. SPEX allows converting a model photon spectrum into the count spectrum with the use of the spectral response matrix and comparing it with the observed spectrum by adjusting model parameters, e.g., temperature, and minimizing χ^2. It was assumed in the model employed by Battaglia at al. [51] that flare radiation consists of two isothermal components with temperature T_1 and emission measure EM_1 and T_2 and EM_2, respectively, plus a nonthermal component. The model permits adjusting nine free parameters, four of which determine emission measure and the temperature of the two thermal components, while the five others are responsible for the characteristics of the nonthermal component. Such a large number of parameters made it possible to accurately describe the shape of the experimental RHESSI spectra (Fig. 6), including such features of theirs as discontinuities of the spectrum in the low energy E_{turn} and high energy E_{br} regions.

To construct the desired dependence between flare classes and their plasma temperature, the authors of [51] compared the SXR radiation flux recorded by GOES and T_1 values obtained by analysis of RHESSI spectra. The resulting dependence proved significantly different from that derived earlier by Feldman et al. [48]. However, it can be just as well approximated by the exponential function and demonstrates a principle effect, a drop in plasma temperature when the flare class is downgraded. Doubtless, the main cause of the discrepancy between the results of Feldman's work and Battaglia's study is the use of different methods for temperature measurement. The data obtained by Battaglia et al. are graphically presented in Fig. 8 below together with results of other publications cited in this section.

Hannah et al. [55] reported results of a statistical analysis of 25,705 weak flares of A to C classes making use of RHESSI data and the CHIANTI atomic database, version 5 [56, 57]. Apart from that, their spectrum processing methods for determining temperature and emission measure were analogous to those of Battaglia et al. [51]. The dependences of plasma temperature on flare power obtained in [55] were similar to those derived by Feldman and co-workers [48].

In an analogous study by Li et al. [58], the authors considered 1843 flares of C1 and higher classes based on

RHESSI and GOES data. Both the temperature and the emission measure were determined at the maximum of an SXR radiation flux using the standard procedures for the treatment of GOES data (see, e.g., [59]). Similar to the aforementioned studies, it was shown that temperature grows exponentially with the enhancement of the SXR radiation flux.

A sample of 50,000 events of X-ray flare classes B to X was analyzed by Ryan et al. [60] using the GOES data. A special algorithm was developed allowing the background subtraction procedure and temperature and emission measure determination to be significantly improved. The authors showed that simple subtraction of the pre-flare background level frequently leads to marked signal distortions, especially when flare time profiles overlap. A number of criteria for the choice of the background level were formulated, with the data being analyzed simultaneously in two channels (0.5–4 and 1–8 Å) of the GOES X-ray monitor. Unlike the authors of other studies in which all the parameters of interest were determined at the same point in time (the moment of soft or hard X-ray emission flux maximum), Ryan et al. analyzed the entire flare time profile and chose maximum values of each parameter, regardless of the instant at which a maximum was reached. Similar to other works, the obtained dependences of temperature and emission measure on SXR radiation flux proved to fairly well agree with exponential and power functions, respectively.

Caspi et al. [61] considered correlations of temperature and emission measure with a hot plasma SXR radiation flux for 37 large flares of M and X classes. Plasma parameters were determined from the RHESSI data by a method analogous to that employed by Hannah et al. [55]. The study confirmed the dependence between maximum plasma temperature and the X-ray class of the event described by the power function. The authors constructed an analogous dependence for temperatures based on the GOES data and found that the resulting function proved less steep than in the case when temperature was measured using the RHESSI data. This instrumental effect was attributed to reduced RHESSI sensitivity to low-temperature radiation responsible for the overestimated mean temperature of the plasma.

The high power of the studied events of A and higher classes significantly limited the above studies, which made impossible a reliable conclusion about the dependence of temperature on the flare class for micro- and nanoevents. Moreover, it was shown (see, for example, the results of Feldman et al. in Fig. 5) that if the dependences obtained in these studies were extended to the low-temperature region, the temperature became zero, even for A1 class flares. In other words, extrapolation of temperature dependences for large flares to the region of low-energy flares gives evidence of the impossibility of effective plasma heating in micro- and nanoflares.

This observation gap was filled by Kirichenko and Bogachev [62], who analyzed a large sample of solar microflares that included 481 events ranging from class B to A0.01, i.e., two orders of magnitude below the GOES classification threshold. The possibility of studying such weak events was ensured by a combination of favorable observation conditions (the deep solar activity minimum of 2009) and specific features of the instrumentation employed to investigate flare characteristics based on the results of X-ray spectrophotometry with the use of the Solar PHotometer IN X-rays (SPHINX) [63], which had a sensitivity threshold two orders of magnitude lower than that of GOES and was operated as a component of TESIS [42, 64] aboard the CORONAS-Photon satellite [65]. The data obtained were additionally verified using the information yielded by the TESIS MgXII Imaging Spectro-Heliometer (MISH) with a temperature recording threshold of $(3.5-4)\times 10^6$ K. The very fact that microflares were registered on a MISH image suggested plasma heating up to at least 3.5×10^6 K.

Kirichenko and Bogachev estimated plasma temperature by approximating thermal radiation spectra of the flares measured by SPHINX in the framework of the two-temperature approximation with the use of the CHIANTI atomic database [56, 66]. The model approximation of the SPHINX spectrum is exemplified by Fig. 7.

The principal objective of Kirichenko and Bogachev's work was to continue identification of dependences between low-energy flare temperature and power observed in earlier studies. One of the dependences thus obtained together with the superimposed results of the publications cited above [48, 51, 55, 58, 60, 61, 64] is presented in single-temperature (Fig. 8a, b) and two-temperature (Fig. 8c, d) approximations. The red squares denote the set of observations performed by Kirichenko and Bogachev (each square corresponds to one flare). The red lines are two linear approximations of these data, one for low-power flares of X-ray classes below A1.0, the other for high-power flares above A1.0. Lines of different colors indicate data from other authors.

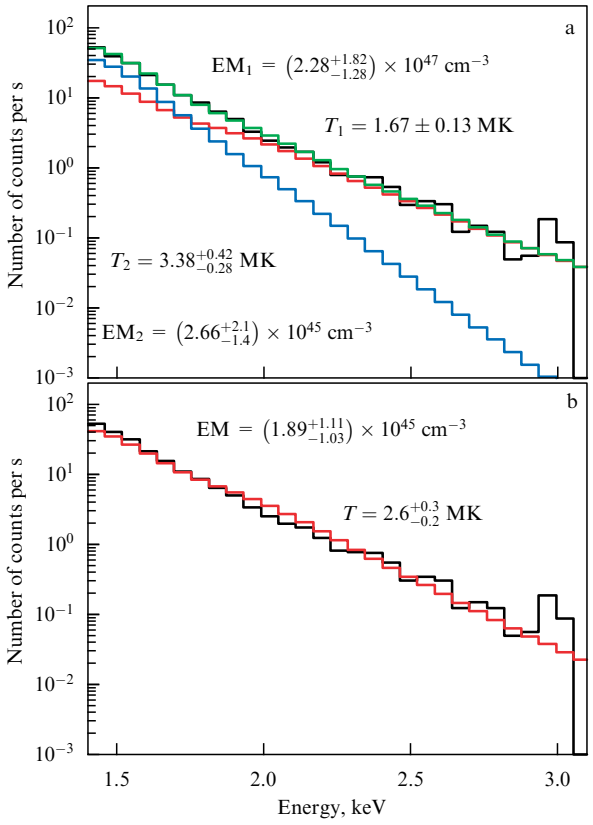

Figure 7. (Color online.) Example of microflare temperature determination from the thermal radiation spectra measured by SPHINX. Black line — experimental spectrum, (a) two-temperature approximation (blue and red lines correspond to the model spectra for temperatures T_1 and T_2; green line — integral model spectrum without temperature separation. (b) Single temperature approximation (red line corresponds to the model spectrum for temperature T).

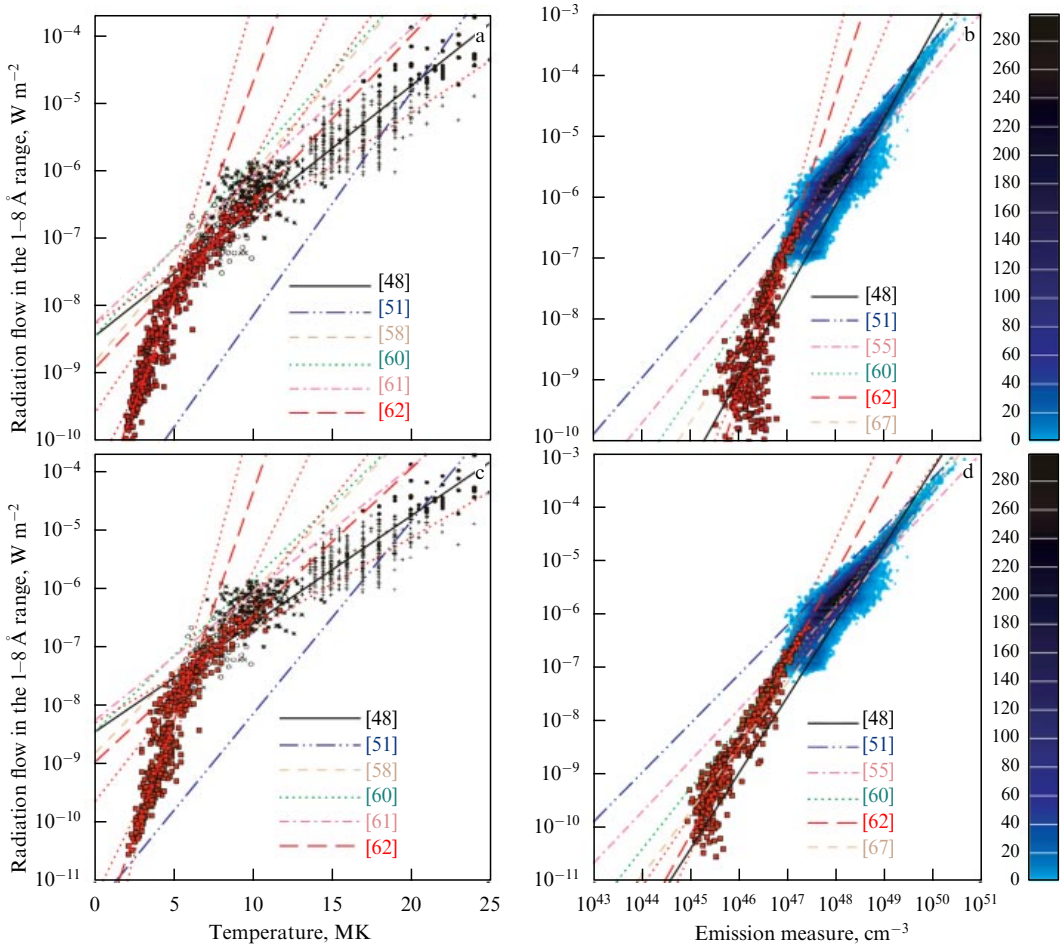

Figure 8. (Color online.) Dependence of SXR flare emission flux in the 1–8-Å range on flare plasma temperature (a, c) and emission measure (b, d) obtained by Kirichenko and Bogachev [62]. Red squares indicate TESIS experiment data. Red dotted lines are their approximations for the flares of X-ray classes below and above A1.0. Figures a and b show results obtained in the framework of the isothermal model; Figs c and d show results obtained within the two-temperature model. Black symbols indicate data obtained by Feldman et al. [48]. Blue two-dimensional histograms are data from Ryan et al. [60]. Different kinds and colors of lines show approximations of the data from [48, 51, 55, 58, 60, 61, 67] in accordance with the figure legend.

For flares class above A1.0, the linear correlation between temperature T and the logarithm of SXR radiation flux F was obtained based on the data of Refs [48, 51, 55, 58, 60, 61, 64]:

$$\log_{10} F = a + bT. \qquad (13)$$

As was noted in a preceding paragraph, extrapolation of these dependences to the low-energy flare region suggested the impossibility of plasma heating in events lower than A1.0 classes. Direct examination of A0.01–A1.0 class flares showed that such extrapolation is incorrect, and the relationship between an SXR radiation flux and flaring plasma temperature for low-energy flares is more complicated. The set of data can be differentiated into two parts with different slopes, below and above the A1.0 level. Figures 8a and 8c describing microflares demonstrate steeper sloping than Figs 8b and 8d related to ordinary flares.

The $F(T)$ dependence can be approximated by the same function over the entire power range, from A0.01 and above, if the power function in the form

$$\log_{10} F = a + b \log_{10} T \qquad (14)$$

is used instead of the logarithmic one. This approximation is presented in Fig. 9. Evidently, an approximation using formula (13) requires different slopes for the flares below and above A1.0, as shown in Fig. 8. At the same time, an approximation by the power function (14) uniformly describes flares over the entire range of interest, from A0.01 to higher classes.

The study showed that dividing the model into single- and two-temperature models does not make much sense for flares of A1.0 and higher classes, because the results of both models are practically identical, in contrast to a significant difference for weak events of lower classes. The discrepancy can be accounted for by an observation suggesting that a decrease in the flare power reduces the relative contribution of the high-temperature component to the formation of integral flare radiation. For flares of A, B, and higher classes, an SXR radiation flux formed by the high-temperature component is 2–4 orders of magnitude higher than that generated by the low-temperature component. In this sense, separation of radiation into two temperature components does not significantly change the results of modeling. For microflares below A1.0, radiation from the low-temperature component is comparable to that from the high-temperature one; both radiation spectra need to be approximated by two components.

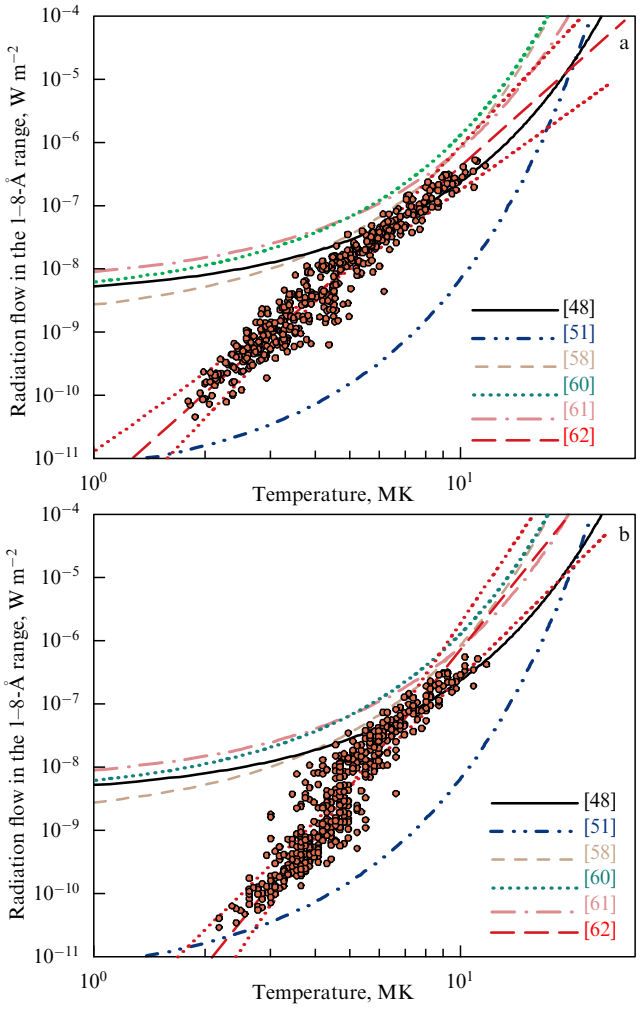

Figure 9. (Color online.) Approximation of the temperature dependence of SXR radiation flow $F(T)$ by the power function: (a) single-temperature approximation, (b) two-temperature approximation. The notations are analogous to those in Fig. 8.

The fact that a decrease in flare power causes a reduction in the relative contribution of the high-temperature component to the formation of integral radiation implies the existence of a minimal class of flares such that all lower class flares are devoid of high-temperature plasma. In the framework of the two-temperature model, this corresponds to a case in which the temperature of the hot component T_2 becomes equal to that of the cold one T_1. Figure 10 presents some results of the study carried out by Kirichenko and Bogachev [62]. The T_2/T_1 ratio measured for the flares is plotted on the abscissa and the SXR radiation flux of a flare in the 1–8-Å range, i.e., its X-ray class, on the ordinate. An analysis of this dependence shows that the ratio $T_2/T_1 = 1$ is reached when the SXR radiation flux is

$$F_1 = 10^{-11.71\pm0.77} = 1.9 \times 10^{-12}\ \mathrm{W\,m^{-2}}\,, \qquad (15)$$

belonging to the A0.0002 class, i.e., four orders of magnitude below A1.0, which may correspond to flares with energies of $10^{24} - 10^{25}$ erg (the lower boundary of the nanoflare range), leaving open the possibility of plasma heating over the entire range of events currently accessible to observation, from ordinary flares to micro- and nanoevents. Note that tempera-

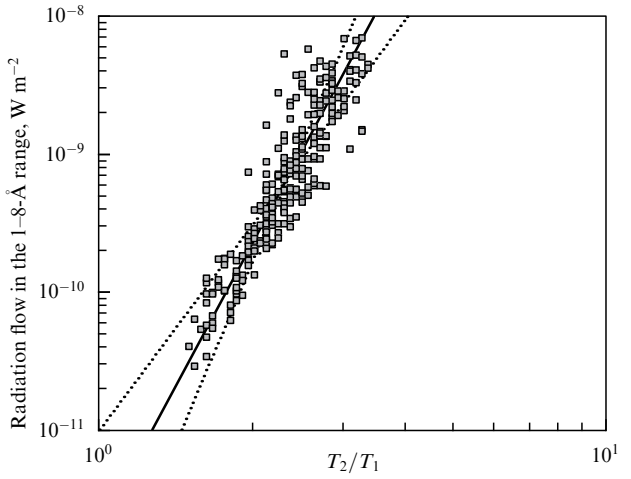

Figure 10. Microflare SXR radiation flow as a function of the ratio of temperatures of flaring and surrounding plasmas on a log scale.

tures at this point,

$$T_1 = T_2 = (1.66 \pm 0.34) \times 10^6\ \mathrm{K}\,, \qquad (16)$$

on the whole correspond to the coronal plasma temperature of $(1-2) \times 10^6$ K.

4. Magnetic reconnection in small-scale solar flares and structures

Detailed studies of small-scale solar flares are mainly hindered by the limited resolution of observations. This may not seem relevant at first to the time resolution. Indeed, measurements of solar radiation flux in the UV and soft X-ray bands can be obtained with a cadence of less than 1 s or even in the single photon counting mode. Such accuracy would certainly be sufficient for a detailed study of temporal profiles of micro- and nanoflares. However, the contribution of such flares to the total solar radiation flux is negligible due to their low energies, which makes their identification and examination problematic. For this reason, image processing rather than total flux measurement is the main method for studying low-energy flares. A group of pixels corresponding to the core of the flare is identified in the images of the Sun, and the signal is further investigated only in these pixels. Temporal resolution of solar imaging is much lower compared to that of total flux measurements. For example, the cadence of AIA/SDO observations is typically 12 s [68]. The temporal resolution achieved in the TESIS experiment on board the CORONAS-Photon satellite is 4 s, which appears to be the best value obtained so far for the EUV range (see, e.g., [43, 69]). However, only a few hundred images were obtained this way.

As far as spatial resolution is concerned, the diffraction limit in the EUV spectral range has not yet been reached, the main limitation being the size of detector pixels. Complementary metal-oxide-semiconductor (CMOS) matrices and back-illuminated charge-coupled devices (CCDs) are commonly used as detectors. The respective limitation for TESIS telescopes is 1.7″ per pixel. For the AIA, each pixel corresponds to 0.6″ or roughly 440 km on the Sun. The highest angular resolution reached so far is that of the Hi-C [71] sounding rocket experiment (0.25″) and of the Interface

Region Imaging Spectrograph (IRIS) [70] (around 0.35″), which, however, is obtained only for a limited field of view. Observations show that even such high resolution is insufficient to resolve the spatial structure of nanoflares. Therefore, they have to be studied as point-like structureless objects.

The lack of information about the structure of nanoflares poses a question as to why these events are generally regarded as flares, given that other mechanisms for energy release in the corona exist, such as small-scale plasma heating by drift currents [72]. Moreover, observations show small-scale phenomena of a hydrodynamic nature to be present on the Sun, such as macrospicules and small-scale prominences [73–75]. Under such conditions, when the accuracy of observations is not enough to confirm the flaring nature of an event, indirect signatures become of greater importance. The most essential of them are the changes in the magnetic field near the area of energy release that are specific to solar flares. A solar flare is known to result from a burst-like release of the energy previously accumulated in the strong magnetic field concentrations. It is generally believed that the initially potential (without currents) magnetic field configuration on the Sun becomes progressively more complicated with time under the action of photospheric plasma motions or as a result of the emergence of new magnetic flux. The interaction of oppositely directed magnetic fields generates electric currents (typically in the form of current sheets) which introduce additional energy — the so called free energy — relative to that of the initial potential structure. The currents lose stability after they reach a certain magnitude and the magnetic configuration rapidly returns to the initial potential state with the impulsive release of the accumulated free energy. Thus, a solar flare occurs (see, for example, [16, 76, 77]).

The extension of this standard model to low-energy flares gives rise to the assumption that the change of magnetic field should be observed in their vicinity either preceding or simultaneous with a flare which results from an explosive rearrangement of the magnetic field configuration. Another indirect sign of the flaring nature of the compact emission sources in the corona could be their spatial correlation with complex (dipole and quadrupole) magnetic structures.

The coincidence of nanoflares with the sites of magnetic field concentration was noted as early as 1988 by Parker, who pointed out that the corresponding bursts of emission coincide with small isolated magnetic dipoles [1]. However, the standard solar flare concept does not provide for the possibility of energy release in dipole structures (with one N-center and one S-center), because oppositely directed magnetic fields do not interact in such structures. To resolve this problem, Parker assumed that the reconnection of magnetic lines occurs as a result of magnetic field braiding by photospheric convective motions of the plasma [1, 14, 78, 79]. Numerical simulations show that current sheets formation and reconnection are possible by this mechanism with subsequent energy release (see, e.g., [80–84]) with the power-law energy distribution of nanoflares [85]. Naturally, no plausible experimental confirmation of this mechanism could be obtained in the late 1980s.

The main difficulty encountered in the study of magnetic structures in the vicinity of nanoflares is the same one that complicates an analysis of nanoflares themselves — the corresponding structures are very small-scale. Moreover, observing coronal magnetic fields remains in fact an unresolved problem [86–88]. The most convincing evidence of a reconnection in braided magnetic lines in the corona at very small scales was provided by the Hi-C sounding-rocket observations of the Sun that revealed signs of energy release in braided coronal loops [89–92]. These results, however, can be debated because of the limited spatial resolution of observations. Some authors argue that the observed radiation sources are not directly associated with the field line braiding sites and heating is homogeneous over the entire loop length [93]. Moreover, there is evidence that the structures observed with extremely high spatial resolution of Hi-C are actually cold loops with a temperature below 10^6 K, while the high-temperature loops heated as a result of magnetic reconnection can not be seen even at such a high resolution [94–96], which questions the very fact of their existence.

This accounts for the growing popularity of the classical reconnection mechanism with energy released by the interaction of oppositely directed magnetic loops with the formation of zero points [97–99], in contrast to energy release resulting from braiding of magnetic field lines. Another signature of this mechanism can be the magnetic flux cancellation at the photosphere. Recent observations of the Sun show that flux cancellation is universal and can provide energy needed for the formation of a large number of compact radiation sources [100]. There is also evidence that both mechanisms may operate simultaneously. For example, the reconnection resulting from flux cancellation can trigger reconnection in overlying braided field lines [101].

At present the question is widely discussed that one of the most reliable evidence of small-scale magnetic reconnection is so-called Ellerman bombs, discovered almost 100 years ago [102] as a characteristic change in the shape of the hydrogen spectral line H_α (enhanced brightness of the line wings with simultaneous darkening in the line center). Modern imaging observations of the Sun show that Ellerman bombs are actually small-scale flare-like radiation sources 800–1000 km in size [103, 104] formed in the lower layers of the chromosphere just above the photosphere [105]; hence, their phenomenological difference from nanoflares that occur in the corona.

Spectral analysis shows that Ellerman bombs are associated with plasma heating by 200–1500 K [106–109], i.e., much weaker than during coronal nanoflares, when the plasma temperature increases by a few hundred thousand K. The energy released in Ellerman bombs corresponds to that at the upper boundary of the nanoflare range ($10^{26}-10^{28}$ erg) [107, 108, 110]. The energy spectrum is power-law with exponent 2.1 [110].

Whether Ellerman bombs are a chromospheric analog of coronal nanoflares remains an open question, despite a degree of similarity between them. Some observations appear to give evidence of the formation of UV radiation bursts in Ellerman bombs, besides optical radiation, which suggests heating of part of the material up to the temperature of the transition region, $2 \times (10^4-10^5)$ K [103, 111–114]. It is doubtful, however, whether these bursts are a counterpart of Ellerman bombs or just a spurious coincidence, because the available numerical models can reproduce either Ellerman bombs or bursts of UV-radiation but not both at a time [115–118]. The main problem is that the precise mechanism of energy transfer from the photosphere and the lower chromosphere to upper layers remains elusive [111, 119].

Let us return to observations of the magnetic field. It was shown that Ellerman bombs are formed near the neutral line of magnetic dipoles [103, 120], usually at the moment of the emergence of new magnetic flux [121, 122], or alternatively during the cancellation of opposite magnetic flux polarities [108, 109, 123, 124]. The whole picture resembles that of a solar flare. No wonder most authors consider magnetic reconnection as a source of the Ellerman bomb energy (see, for instance, [126]), although purely hydrodynamic models of Ellerman bomb formation exist (see [125]). Today, the following scenario is generally accepted. Ellerman bombs appear where the upper parts of undulatory magnetic flux tube formed due to Parker instability emerge in the photosphere [127, 128]. According to calculations, relaxation of this structure results in the reconnection at the dips of the undulating flux, visible as the convergence of loop footpoints and subsequent cancellation of magnetic flux in the photosphere [119, 129, 130]. It was shown that such reconnection proceeds most efficiently in the temperature minimum region of the lower chromosphere [131].

Another type of compact sources in the Sun's atmosphere is represented by coronal bright points [132], discovered in the early 1970s in solar images taken in the X-ray wavelength range (for this reason, they were referred to as X-ray bright points for nearly 20 years [133]). The coronal bright points are observed not only in the X-ray wavelength range but also in the EUV [134–136] and radio-frequency ranges [137–140]. Their structure includes a core about 5 thousand km in size surrounded by a diffuse radiation area measuring 10–30 thousand km [25, 137, 138, 141–143]. High angular resolution observations reveal a system of two or three small-scale loops (12×2.5 thousand km) in this region [134, 144–146]. The mean lifetime of coronal bright points is estimated at approximately 8–20 h [25, 142, 147]; their distribution pattern is dominated by events having shorter lifetimes [143, 148]. Thus, the size and the lifetime of these events are close to the respective parameters of solar supergranules [149].

Investigations into energy characteristics of coronal bright points demonstrated that the plasma in them can be heated up to $1.1-3.4 \times 10^6$ K [25, 140, 150, 151], even if part of it exists at lower temperatures of around $5 \times 10^4 - 5 \times 10^5$ K [137, 138, 140]. The temperature distribution shows a minimum near $(2-3)\times 10^5$ K corresponding to the maximum of the radiation loss function in the corona; the temperature of certain points does not reach coronal values at all [141, 152–154]. Numerous observations showed that rapid changes in radiation intensity at a time scale on the order of several minutes [25, 155–159] are accompanied by variations in plasma temperature and a substantial rearrangement of the visible structure. Bursts of radiation in the corona are followed, with a delay of several minutes, by brightenings at loop footpoints in chromospheric transition-region spectral lines [160, 163], with heat conductivity playing the key role in the energy transfer mechanism [141, 156, 164]. Such behavior of the coronal bright points is fairly well described by the model of impulsive loop heating due to magnetic reconnection [151, 160, 164, 165].

The very first observations of coronal bright points showed that they are almost invariably associated with small dipole concentrations of the photospheric magnetic flux [26, 166–169], even if a more complicated field configuration may sometimes be visible [170]. The corresponding magnetic flux is usually of the order of $10^{18} - 10^{20}$ Mx [25, 136, 171], while the lifetime and intensity of coronal bright points as a rule increase with increasing total magnetic field flux [26, 136, 146, 158] and weakly depend on its topology [141, 172]. The thermal energy released in coronal bright points amounts to $4.5\times 10^{28} - 2.7\times 10^{29}$ erg and fairly well correlates with the magnetic field energy, which provides indirect evidence that the field serves as its main source [156]. Extrapolation of the magnetic field to the corona in the potential approximation is in excellent agreement with the real loop structure seen in images, which suggests the largely potential character of the field [136, 146, 150, 162, 163].

Observations of magnetic field evolution show that most coronal bright points (around 70–80%) are associated with a cancellation of photospheric flux concentrations of opposite polarity [139, 150, 172, 173], while the remaining bright points are related to the emergence of new magnetic dipoles [26, 135] that can be just as well followed by flux cancellation [147]. Model studies confirm that the change in magnetic configuration due to flux cancellation can provide enough energy for heating [174–176]. The significant correlation between radiation intensity of coronal bright points and the magnetic flux cancellation rate also proves the validity of this mechanism [150, 156, 157]. The possibility of interaction between emerging small-scale magnetic features and the surrounding large-scale structure was considered in [136, 161, 177, 178]. It is associated with reconnection in the magnetic separator region, accompanied by energy release [171, 179]. A two-step process probably takes place in which the initial homogeneous plasma heating due to magnetic flux cancellation is followed by a drastic heating up to coronal temperatures owing to reconnection at the separator [155, 180, 181]. Taken together, observations of coronal bright points argue in favor of the classical scenario of magnetic reconnection in small-scale loops as opposed to the Parker scenario, assuming reconnection of braided magnetic field lines.

One of the strongest observational evidence in favor of the classical scenario of magnetic reconnection in coronal nanoflares has recently been reported by Ulyanov et al. [182]. The authors used data from the AIA/SDO [182] to examine a quiet-Sun area on the solar disk 5×5 angular minutes in size in the 131 Å, 171 Å, and 193 Å channels showing hot coronal plasma with a temperature of about 10×10^6 K, 0.7×10^6 K, and 1.5×10^6 K, respectively. A few hundred statistically significant small-scale radiation bursts were registered during 6 h of observation. The statistically most meaningful event (Fig. 11a–c) was chosen for comprehensive analysis using magnetograms from the SDO/HMI (Helioseismic and Magnetic Imager) (Fig. 11d). The total thermal energy of the event was found to be 6×10^{25} erg, which allowed it to be classified as a medium-size nanoflare.

The source thus found could be observed simultaneously in the three channels. It was situated in the upper part of a compact system of coronal loops extending over 20 thousand km and therefore corresponded to the characteristic structure of larger flare events [16], even if on a smaller scale. The intensity profile presented in Fig. 12 exhibits three major peaks having a total duration of around 30 min within which smaller peaks of a higher frequency are seen. Such a profile suggests the impulsive character of plasma heating in the nanoflare. Plasma temperature in the flare maximum deduced from the ratio of intensities in the 171 Å and 193 Å channels is 3.1×10^6 K; hence, the flare thermal energy can be estimated at 6×10^{25} erg.

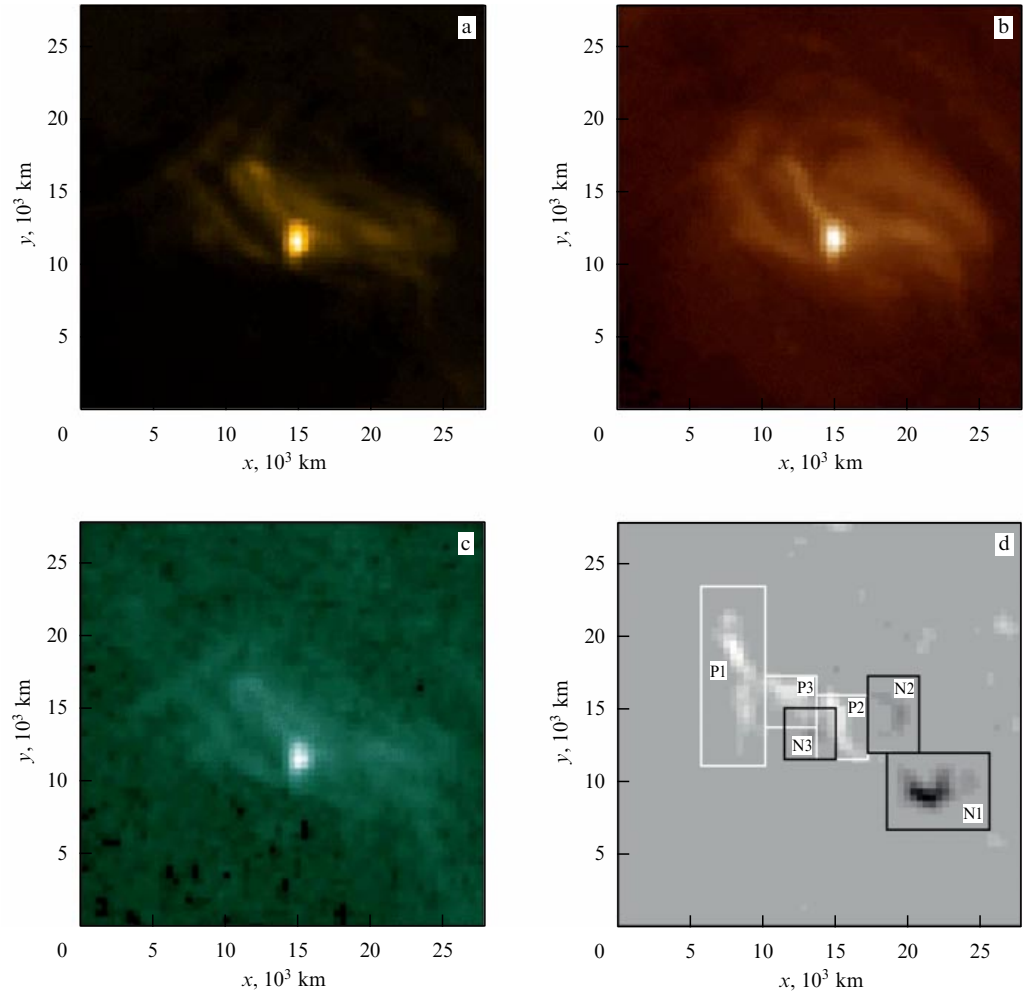

Figure 11. (Color online.) Images of the nanoflare simultaneously taken in the 171 Å (a), 131 Å (b), and 193 Å (c) channels of the AIA and the respective magnetogram produced by the Helioseismic and Magnetic Imager (HMI) (d) (from [182]). Rectangles in panel (d) mark the locations of positive, P1–P3, and negative, N1–N3, magnetic flux concentrations.

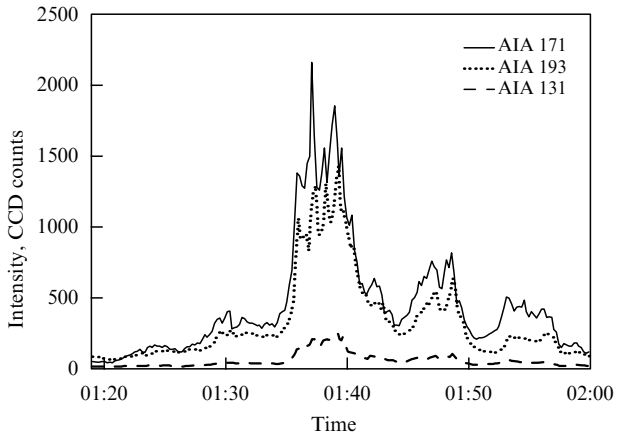

Figure 12. Nanoflare radiation profile measured in three AIA channels: 171 Å (solid line), 193 Å (dotted line), and 131 Å (dashed line). (From [182].)

Analyzing the series of magnetograms allowed, despite their relatively low spatial resolution, to identify several magnetic field concentrations (Fig. 11d) that were used to reconstruct magnetic field topology in the vicinity of the nanoflare before, during, and after the observed burst of radiation (Fig. 13). It was shown that the energy release in the corona was initiated by the emergence of P3–N3 magnetic dipole (Fig. 13) that disturbed the initial structure of the region. After the nanoflare, the magnetic structure relaxed back to a dipole without loss of the strongest magnetic concentrations P1 and N1. Such a scenario reproduces in detail the classical flare scenario. Although shear displacements of magnetic loop footpoints frequently trigger the energy release in large flares [183], in this case the absence of such motions was shown.

The free energy accumulated due to the emergence of the P3–N3 flux amounted to 8.9×10^{25} erg (as determined by the nonlinear force-free field (NLFFF) extrapolation method in the corona [184]), which means that roughly 2/3 of this energy was converted into plasma thermal energy (a highly unusual finding for large flares in which not more than 10% of the energy is normally spent to heat plasma). The energy accumulation process occurred as an enhancement of electrical current in the corona (see Fig. 14 for its spatial density distribution). The highest current density was reached at 15,000 km above the photosphere, the size and position of the current density concentration center coinciding with those of the nanoflare emission source.

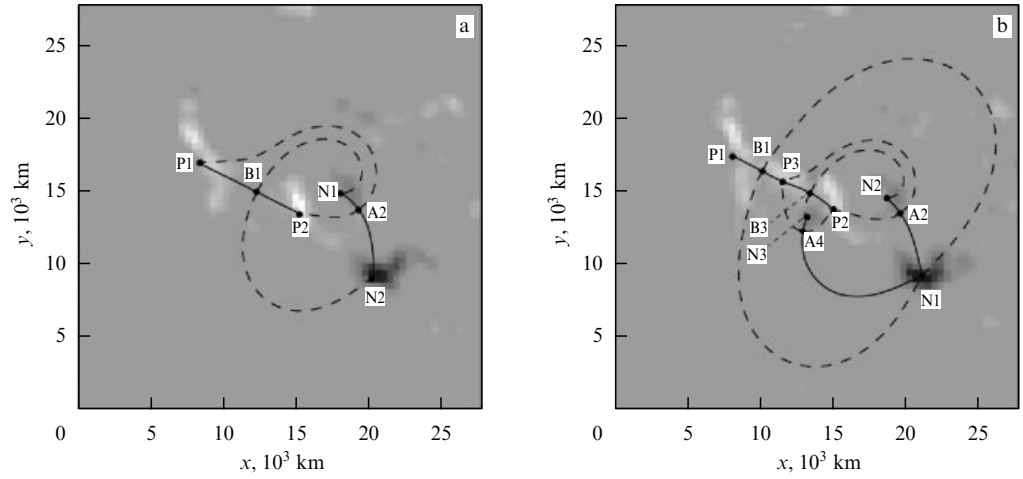

Figure 13. Magnetic field configuration in the corona directly before (a) and immediately after (b) the nanoflare [182].

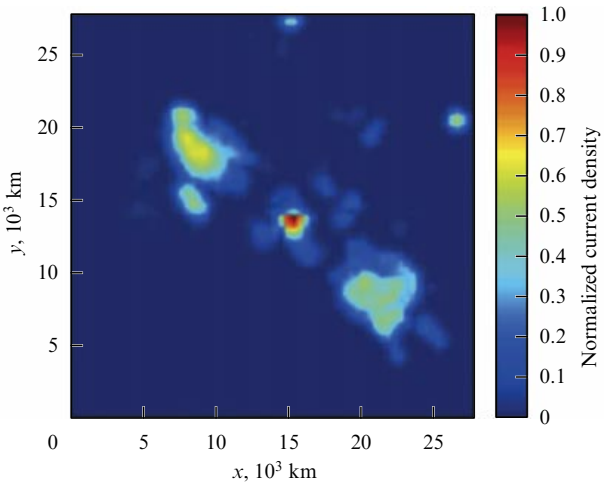

Figure 14. (Color online.) Electric current distribution in the corona during the nanoflare at an altitude of 1.5 thousand km determined based on the nonlinear force-free field extrapolation. (From [182].)

5. Low-energy flares in active regions

Considering low-energy flares traditionally implies reconnection in small-scale magnetic fields arising from field line interlacing by convective surface plasma streams or from the emergence of small-scale magnetic fluxes. At the same time, the formation of micro- and nanoflares in large-scale magnetic fields (active solar regions) is not fundamentally forbidden. A large-scale regular structure of the magnetic field in such regions may co-exist with small-scale patterns of more complicated topology in which local energy release occurs in the form of small-scale flares. The main obstacle to observing such events is the high level of background radiation in large active regions against which it is difficult to distinguish small flares, because their registration is hindered by the presence of ordinary flares.

The formation of micro- and nanoflares in large active regions is indirectly evidenced by a change in the radiation structure leading to an unaccountable rise in SXR radiation, which suggests plasma heating. Of special interest are cases in which the active region has a simple (monopole or dipole) structure, making large-scale reconnection impossible.

The identification of the high-temperature part of the radiation spectrum of active regions is seriously complicated by the wide temperature response range of the instruments used for the purpose, such as AIA telescopes carried by the SDO spacecraft [68], which are currently the major space tool for Sun exploration, or the X-ray Telescope (XRT) aboard the Hinode satellite [185]. The high-temperature radiation component visible in images is blended with low-temperature background. Synthetic images in which high- and low-temperature components are separated by model methods (see [186–188]) suffer a considerable error that prevents unambiguous discrimination between the part of the high-temperature signal formed by a hot plasma and that resulting from algorithm imperfections.

Most currently available XRT observations of a high-temperature plasma [189–192] relate to large active regions with high flare activity. As far as high-temperature radiation from nonflaring active regions is concerned, it was shown by some authors that synthetic methods for recording the high-temperature plasma are, in principle, insensitive to such radiation if it is below a certain threshold level. For example, the data obtained by the XRT [193] indicate that the high-temperature component (over 4×10^6 K) of radiation is observed only when its emission measure exceeds 0.1 of the background one formed by the plasma with $T \approx (2-3) \times 10^6$ K. Of course, this seriously hampers assessment of the weak contribution from micro- and nanoflares.

A more promising approach appears to be quasi-monochromatic observations with signal registration in such a narrow transmission band that it can be regarded as related to a single spectral line at which a given range is centered. Such observations in the hard X-ray radiation wavelength range were performed using the Nuclear Spectroscopic Telescope Array (NuSTAR) [194, 195] and Focusing Optics X-ray Solar Imager (FOXSI) [196, 197]. Analogous studies in the soft X-ray radiation wavelength range were carried out with the use of the Flat Crystal Spectrometer (FCS) [198] aboard the SMM spacecraft, the SPHINX spectrophotometer [199, 200], the REntgenovsky Spectrometer s Izognutymi Kristallami (RESIK) [201, 202], the MISH imaging spectroheliometer [203] of the CORONAS-Photon satellite, the Solar Ultraviolet Measurement of Emitted Radiation spectrometer (SUMER) [204, 205], and the Extreme Ultra-

Table 2. Observations of hot plasma in a non-flaring active regions. DEM_X — differential emission measure for $X \times 10^6$ K.

Instrument	Range	DEM_5/DEM_3	DEM_{10}/DEM_3	References
SUMER	Fe XIX 1118 Å	$\leqslant 0.1\%$	$\leqslant 0.1\%$	[204]
FCS/SSM	13–20 Å	$\leqslant 1\%$	—	[198]
NuSTAR	2–78 keV	$\leqslant 10\%$	$\leqslant 0.1\%$	[194]
FOXSI	6–8 keV	$\leqslant 3\%$	$\leqslant 0.003\%$	[196]
SPHINX	1.34–7 keV	—	—	[199]
EUNIS-13	Fe XIX 592.2 Å	—	$\leqslant 7.6\%$	[206]
RESIK	3.4–6.1 Å	$\leqslant 0.1\%$	—	[201]
XRT	2–40 Å	$\leqslant 10\%$	$\leqslant 10\%$	[193]
AIA	94 Å	$\leqslant 1-10\%$	$\leqslant 1-10\%$	[187]
MgXII/SPIRIT	Mg XII 8.42 Å	$\leqslant 0.01\%$	$\leqslant 0.001-0.01\%$	[203]

violet Normal Incidence Spectrograph (EUNIS-13) [206] operating in the EUV wavelength range.

The main characteristic of the temperature structure of active range radiation is the differential emission measure determined from the equation

$$\mathrm{DEM}(T) = n^2 \frac{\mathrm{d}V}{\mathrm{d}T}. \tag{17}$$

The higher the DEM for a concrete temperature value, the larger the plasma fraction that has this temperature. In other words, determining the DEM ratio at different T allows a conclusion on the relative content of plasmas with different temperatures in a concrete active region. Such characteristic T values can be 3×10^6 K (characteristic background temperature of the active region), 5×10^6 K (high-temperature plasma), and 10×10^6 K (flare plasma). The respective DEM ratios, viz. DEM_5/DEM_3 and DEM_{10}/DEM_3, obtained in different experiments are presented in Table 2.

Below we present some comments to aforementioned studies.

The data for hard X-ray radiation are taken from the work of Hannah et al. [194], who explored the non-flaring activity region based on NuSTAR observations and estimated plasma temperature at roughly 3×10^6 K. Also used were results by Ishikawa et al. [196], who analyzed FOXSI missile experiment findings [197], where pictures of the Sun were obtained by grazing incidence focusing optics. Ishikawa failed to register a signal in the active area of interest and used this observation to estimate the upper threshold for the amount of hot plasma in the absence of flares.

Del Zanna et al. [198] examined SXR radiation spectra of six unperturbed active regions obtained using a FCS/SMM spectrometer in the 13–20-Å wavelength range. Results of these observations allowed the conclusion that the emission measure of a high-temperature plasma must not exceed 2×10^{27} cm^{-5}. The authors of [199] analyzed X-ray spectra registered by a SPHINX spectrometer during two weeks. Time intervals during which the solar flare activity was observed were excluded from integration. The synthetic spectrum thus obtained was indicative of X-ray radiation attributable to the presence of a nonflare hot plasma. However, this fact does not provide an unambiguous conclusion that the plasma was formed by low-energy flares and was not a residual product of a higher activity. Sylwester et al. [201] undertook an analysis of the full solar spectrum obtained by RESIK in the 3.4–6.1-Å range and showed that in this case the DEM of the flare-temperature plasma ($\sim 10^6$ K) does not exceed 0.1% of the DEM in the background radiation with a temperature of $\sim 3 \times 10^6$ K. This value can be regarded as the upper estimate of the nanoflare contribution to integral thermal radiation of active regions. Reva et al. in [203] carried out an imaging investigation of the high-temperature non-flaring plasma in the solar corona, making use of the data from the SPectroheliographic soft X-Ray Imaging Telescope (SPIRIT) aboard the CORONAS-Photon satellite [207]. A specific feature of this instrument is insensitivity to plasma temperatures below 4×10^6 K. A significant signal in this temperature region was registered only in post-flare active regions. It was shown, taking account of the instrument's sensitivity, that this finding corresponds to the limitation on the DEM for a nanoflare-produced plasma equaling 0.01% of the DEM of background radiation from active regions.

Table 2 presents the data of Parenti et al. [204] for the EUV spectral region. These authors used the data from the SUMER spectrometer to register a signal in the Fe XIX 1118-Å line coming from nonflare parts of the active region; they interpreted it as proof of high-temperature plasma formation. These data were used to estimate the DEM ratio of the flare-temperature plasma as equaling 0.1% of its background value. Brosius et al. [206] explored the active region in the Fe XIX 592.2-Å line formed at $T \approx 8.9 \times 10^6$ K based on the imaging EUNIS-13 spectrometer data and registered a well apparent signal. Flaring activity was observed in this region at the same period, which was likely to lead to an incorrect estimation of the DEM limitation.

On the whole, the most rigorous constraints on the contribution of nanoflares to the formation of thermal radiation in active regions have thus far been formulated by Ishikawa et al. [196] based on FOXSI imager observations of hard X-ray radiation (no more than 0.003% for the DEM_{10}/DEM_3 ratio) and Reva et al. [203] (no more than 0.001–0.01% based on data for the SXR range).

Cargill [208] simulated heating of the active region plasma by nanoflares, taking into consideration their energy distribution and mean frequency. The resulting temperature and density profiles can be recalculated in terms of differential emission measure to compare them with the above DEM constraints.

Such estimates by Reva and co-workers [203] are presented in Fig. 15, showing that the relative contribution of nanoflares to the formation of high-temperature radiation in an active region rapidly decreases with a rise in their frequency (reduction in time interval τ_N between two successive flares). This seemingly paradoxical observation relates to the general constraint on the integral energy release in nanoflares (see, for instance, Section 1). In light of such a restriction, the higher frequency of the flares implies an energy reduction in each event. A decrease in the power of nanoflares causes, in turn, a reduction in flare plasma temperature (Section 2). If this line

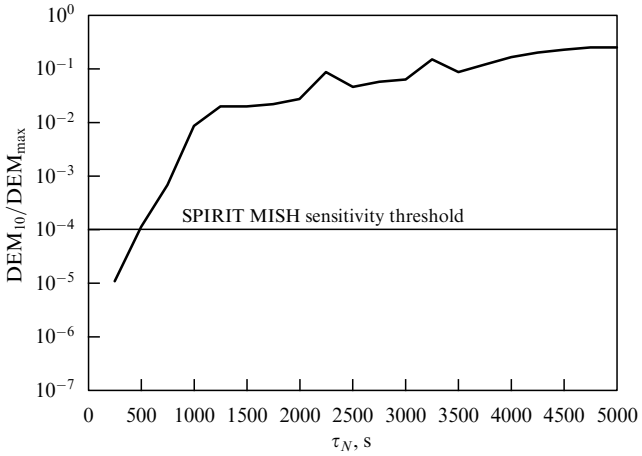

Figure 15. Ratio of DEMs of high-temperature and background (main) plasma components according to results of numerical simulation [208]. (From Reva et al. [203].)

of reasoning and simulation results [208] are on the whole correct, it can be concluded based on the DEM limitations proposed by Ishikawa et al. [196] and Reva et al. [203] ($DEM_{10}/DEM_3 \leqslant 10^{-5}-10^{-4}$) that individual nanoflares in active regions occur at a rate of at least one every 500 s.

6. Conclusion

Results of experimental studies on low-energy solar flares for the last 50 years have brought researchers to a consensus that these events involve a noticeable proportion of the integral energy of solar activity but have failed to answer the question of how large this proportion is. Both experimental estimates and theoretical considerations still leave room for a variety of very extravagant ideas. Some authors argue that solar flares should be regarded as pico- and even femtoevents, the enormous energy of which provides a basis for the solution to all key problems of modern solar physics. According to an alternative opinion, the energy of low-energy flares constitutes but a minor addition to the known large-scale activity and has no appreciable influence on its total balance. None of these concepts can be ruled out based on the currently available information.

Observations leave little doubt about the objective reality of the Sun's microworld. In fact, each advance in the accuracy of imaging observations of the solar corona has led to the discovery of progressively smaller flares and structures. Attempts to integrate these observations into a unified whole demonstrated a virtually identical energy distribution of all kinds of flares in accordance with the power law $dN \sim E^{-\alpha}$. This means that the total energy of solar flares either is limited to $\alpha \leqslant 2$, when the major proportion of the energy is contained in ordinary flares, or grows unrestrictedly at $\alpha > 2$ as E decreases. Because an infinite energy is impossible, there must be such a threshold power of flares (cutoff energy) below which these events are either nonexistent or distributed according to a different law. Experiments demonstrated that the α value is actually very close to 2, being slightly higher or lower depending on the energy assessment method. In other words, there is no definite answer yet. As far as the cutoff energy is concerned, it remains to be discovered in a range of $> 10^{24}$ erg accessible to experimental studies. Blockage of the spectrum at low energies documented in certain experiments is, as a rule, attributable to the limited sensitivity of the instrumentation responsible for the lower than expected number of flares near the sensitivity threshold.

Attempts to elucidate the characteristics of micro- and nanoflares by extrapolation of dependences derived for ordinary events sometimes yield incorrect results. Observations of ordinary flares demonstrate the relationship between their power F and temperature T of the plasma formed in the flares: the weaker the flare, the lower the plasma temperature. The dependence itself is exponential: $\log_{10} F = a + bT$. However, its extrapolation to the low-energy region reveals a plasma temperature tendency toward zero, even for large microflares, at variance with observations. This problem was solved by direct measurements of the $F(T)$ dependence for low-energy flares, which demonstrated its consistency with the power law $\log_{10} F = a + b \log_{10} T$ rather than the exponential one. The dependence for ordinary flares proved to obey the same law, though it was formerly erroneously approximated by the exponential function due to a lack of experimental data. According to these data, plasma ceases to be heated only at a flare power below class $\sim$ A0.0002 corresponding to weak solar nanoflares with an energy of $10^{24}-10^{25}$ erg.

Parker initiated the discussion on the nature and mechanism of energy release that has continued since then, sometimes assuming the most extreme forms up to denial of the outburst nature of nanoflares and attempts to explain them in the framework of hydrodynamic models (without the participation of the magnetic field). In most cases, however, the discussion is centered around the magnetic reconnection scenario. The best known one is the Parker scenario, according to which reconnection occurs as a result of field line interlacing by convective surface plasma streams. An alternative scenario envisages reconnection in small-scale magnetic loops covering the Sun's surface and forming the so-called magnetic carpet. According to this scenario, the mechanism behind the emergence of nanoflares is completely identical to the mechanism underlying the formation of ordinary flares; the two mechanisms differ only in scale.

The answer to the question of how solar flares are actually formed must be sought in experiment. Photography of the corona with a record-breaking angular resolution of 0.25″ during the Hi-C rocket experiment provided evidence of energy release in braided lines of the magnetic field that confirmed Parker's scenario. On the other hand, there is a wealth of information suggesting that nanoflares from as a result of the emergence of photospheric flows. Ulyanov et al. [182] were the first to reconstruct the three-dimensional magnetic field in the vicinity of a coronal nanoflare in 2019 [182]. Moreover, they showed that its dynamics are fairly well described in terms of the ordinary flare scenario.

Thus, the question remains open. The natural suggestion that both scenarios are implemented in the Sun poses new questions, e.g., about the ratio of different flares in the two variants and whether it is correct to combine events of such different natures into a single class of nanoflares. Other scenarios of small-scale energy release in the Sun are feasible. Specifically, observations of large active regions suggest the possibility of formation of flare-temperature plasma ($\sim 10 \times 10^6$ K) in them in the absence of flares, even if in very small amounts. Attempts to apply the nanoflare model to explain this phenomenon have not yet yielded an acceptable result. It was predicted that heating can be due to rather rare (one every 500 s) and therefore large nanoflares,

perhaps unobservable using current instruments. It cannot be ruled out that a different small-scale energy release mechanism operates in this case.

In summary, we are of the opinion that both the nature and the role of low-energy flares still await clarification, despite the progress achieved over the past 50 years. The problem remains the focus of inquiry for solar and space physics. It appears that further advancement in this field is possible only on the basis of new, increasingly more exact, experimental data. We therefore wish every success to foreign space missions, especially those such as the Parker Solar Probe and Solar Orbiter, as well as to Russian ones (the Interhelioprobe and Arka missions) [209, 210, 211]. The last is expected to be the world's first device to produce images of the solar corona with a resolution of 0.1″ or roughly 70 km, hopefully providing convincing detailed experimental data on the nature of small flares and their contribution to the integral coronal activity.

This study was carried out in part (Sections 3 and 4) in the framework of the FSSS-2020-0018 project supported by government funds allocated to winners of a competition for research laboratories of the RF Ministry of Higher Education and Science.

References

1. Parker E N *Astrophys. J.* **330** 474 (1988)
2. Parker E N *Astrophys. J.* **128** 664 (1958)
3. Withbroe G L, Noyes R W *Annu. Rev. Astron. Astrophys.* **15** 363 (1977)
4. Schwarzschild M *Astrophys. J.* **107** 1 (1948)
5. Stein R F, Leibacher J *Annu. Rev. Astron. Astrophys.* **12** 407 (1974)
6. Priest E R *Solar Magnetohydrodynamics* (Geophysics and Astrophysics Monographs, Vol. 21) (Dordrecht: Springer, 1982)
7. Hollweg J V *Solar Phys.* **91** 269 (1984)
8. Davila J M *Astrophys. J.* **317** 514 (1987)
9. Aschwanden M J et al. *Astrophys. J.* **520** 880 (1999)
10. De Pontieu B et al. *Science* **318** 1574 (2007)
11. Nisticò G, Nakariakov V M, Verwichte E *Astron. Astrophys.* **552** A57 (2013)
12. Okamoto T J et al. *Astrophys. J.* **809** 71 (2015)
13. Réville V et al. *Astrophys. J. Suppl.* **246** 24 (2020)
14. Parker E N *Astrophys. J.* **264** 642 (1983)
15. Somov B V, Syrovatskii S I *Sov. Phys. Usp.* **19** 813 (1976); *Usp. Fiz. Nauk* **120** 217 (1976)
16. Somov B V *Plasma Astrophysics* Pt. II *Reconnection and Flares* (Astrophysics and Space Science Library, Vol. 341) (New York: Springer-Verlag, 2007)
17. Lin R P et al. *Astrophys. J.* **283** 421 (1984)
18. Brown J C *Solar Phys.* **18** 489 (1971)
19. Syrovatskii S I, Shmeleva O P *Sov. Astron.* **16** 273 (1972); *Astron. Zh.* **49** 334 (1972)
20. Porter J G et al. *Astrophys. J.* **323** 380 (1987)
21. Blake R L et al. *Astrophys. J.* **137** 3 (1963)
22. Friedman H, in *The Solar Corona. Proc. of Intern. Astronomical Union Symp., Cloudcroft, New Mexico, USA, 28–30 August 1961* (IAU Symp., Vol. 16, Ed. J W Evans) (New York: Academic Press, 1963) p. 45
23. Mandel'štam S L *Space Sci. Rev.* **4** 587 (1965)
24. Beigman I L et al. *Solar Phys.* **9** 160 (1969)
25. Golub L et al. *Astrophys. J.* **189** L93 (1974)
26. Golub L et al. *Solar Phys.* **53** 111 (1977)
27. Canfield R C, Metcalf T R *Astrophys. J.* **321** 586 (1987)
28. Hudson H S *Solar Phys.* **133** 357 (1991)
29. Vaiana G S, Rosner R *Annu. Rev. Astron. Astrophys.* **16** 393 (1978)
30. Krucker S et al. *Astrophys. J.* **488** 499 (1997)
31. Tsuneta S et al. *Solar Phys.* **136** 37 (1991)
32. Berghmans D, Clette F, Moses D *Astron. Astrophys.* **336** 1039 (1998)
33. Delaboudinière J-P et al. *Solar Phys.* **162** 291 (1995)
34. Krucker S, Benz A O *Astrophys. J.* **501** L213 (1998)
35. Aschwanden M J et al. *Astrophys. J.* **535** 1047 (2000)
36. Handy B N et al. *Solar Phys.* **187** 229 (1999)
37. Rosner R, Tucker W H, Vaiana G S *Astrophys. J.* **220** 643 (1978)
38. Aschwanden M J *Solar Phys.* **190** 233 (1999)
39. Kuzin S V et al. *Solar Syst. Res.* **45** 162 (2011); *Astron. Vestn.* **45** 166 (2011)
40. Ulyanov A S et al. *Astron. Lett.* **45** 248 (2019); *Astron. Zh.* **45** 290 (2019)
41. Parnell C C, Jupp P E *Astrophys. J.* **529** 554 (2000)
42. Benz A O, Krucker S *Astrophys. J.* **568** 413 (2002)
43. Aschwanden M J, Parnell C E *Astrophys. J.* **572** 1048 (2002)
44. Saint-Hilaire P, Benz A O *Astron. Astrophys.* **435** 743 (2005)
45. Tsuneta S et al. *Astrophys. J.* **478** 787 (1997)
46. Hannah I G et al. *Astron. Astrophys.* **481** L45 (2008)
47. Glesener L et al. *Astrophys. J. Lett.* **891** L34 (2020)
48. Feldman U et al. *Astrophys. J.* **460** 1034 (1996)
49. Culhane J L et al. *Solar Phys.* **136** 89 (1991)
50. Garcia H A *Astrophys. J.* **420** 422 (1994)
51. Battaglia M, Grigis P C, Benz A O *Astron. Astrophys.* **439** 737 (2005)
52. Lin R P et al. *Solar Phys.* **210** 3 (2002)
53. Schwartz R "Compton Gamma Ray Observatory Phase 4 Guest Investigator Program: Solar flare hard X-ray spectroscopy", Technical Report (Greenbelt, MD: NASA Goddard Space Flight Center Greenbelt, Lab. for Astronomy and Solar Physics, 1996)
54. Smith D M et al. *Solar Phys.* **210** 33 (2002)
55. Hannah I G et al. *Astrophys. J.* **677** 704 (2008)
56. Dere K P et al. *Astron. Astrophys. Suppl. Ser.* **125** 149 (1997)
57. Landi E et al. *Astrophys. J. Suppl.* **162** 261 (2006)
58. Li Y P, Gan W Q, Feng L *Astrophys. J.* **747** 133 (2012)
59. White S M, Thomas R J, Schwartz R A *Solar Phys.* **227** 231 (2005)
60. Ryan D F et al. *Astrophys. J. Suppl.* **202** 11 (2012)
61. Caspi A, Krucker S, Lin R P *Astrophys. J.* **781** 43 (2014)
62. Kirichenko A S, Bogachev S A *Astrophys. J.* **840** 45 (2017)
63. Sylwester J et al. *J. Astrophys. Astron.* **29** 339 (2008)
64. Kuzin S V et al. *Adv. Space Res.* **43** 1001 (2009)
65. Kotov Yu D *Solar Syst. Res.* **45** 93 (2011); *Astron. Vestn.* **45** 99 (2011)
66. Landi E et al. *Astrophys. J.* **711** 75 (2010)
67. Garcia H A, McIntosh P S *Solar Phys.* **141** 109 (1992)
68. Lemen J R et al. *Solar Phys.* **275** 17 (2012)
69. Ulyanov A S, Bogachev S A, Kuzin S V *Astron. Rep.* **54** 948 (2010); *Astron. Zh.* **87** 1030 (2010)
70. De Pontieu B et al. *Solar Phys.* **289** 2733 (2014)
71. Kobayashi K et al. *Solar Phys.* **289** 4393 (2014)
72. Merzlyakov V L *Geomagn. Aeron.* **57** 1063 (2017)
73. Loboda I P, Bogachev S A *Solar Phys.* **290** 1963 (2015)
74. Loboda I P, Bogachev S A *Astron. Astrophys.* **597** A78 (2017)
75. Loboda I P, Bogachev S A *Astrophys. J.* **871** 230 (2019)
76. Priest E R, Forbes T G *Astron. Astrophys. Rev.* **10** 313 (2002)
77. Aschwanden M J *Particle Acceleration and Kinematics in Solar Flares* (Dordrecht: Springer, 2002)
78. Parker E N *Astrophys. J.* **174** 499 (1972)
79. Parker E N *Astrophys. J.* **264** 635 (1983)
80. Wilmot-Smith A L, Pontin D I, Hornig G *Astron. Astrophys.* **516** A5 (2010)
81. Pontin D I et al. *Astron. Astrophys.* **525** A57 (2011)
82. Yeates A R et al. *Astron. Astrophys.* **564** A131 (2014)
83. Hansteen V et al. *Astrophys. J.* **811** 106 (2015)
84. Pontin D I et al. *Plasma Phys. Control. Fusion* **58** 054008 (2016)
85. Knizhnik K J et al. *Astrophys. J.* **853** 82 (2018)
86. Cargill P J *Space Sci. Rev.* **144** 413 (2009)
87. Wiegelmann T, Thalmann J K, Solanki S K *Astron. Astrophys. Rev.* **22** 78 (2014)
88. Fleishman G D et al. *Science* **367** 278 (2020)
89. Cirtain J W et al. *Nature* **493** 501 (2013)
90. Winebarger A R et al. *Astrophys. J. Lett.* **787** L10 (2014)
91. Thalmann J K, Tiwari S K, Wiegelmann T *Astrophys. J.* **780** 102 (2014)
92. Pant V, Datta A, Banerjee D *Astrophys. J. Lett.* **801** L2 (2015)
93. Pontin D I et al. *Astrophys. J.* **837** 108 (2017)
94. Del Zanna G *Astron. Astrophys.* **558** A73 (2013)
95. Aschwanden M J *Astrophys. J.* **874** 131 (2019)
96. Brooks D H et al. *Astrophys. J. Lett.* **772** L19 (2013)

97. Priest E R, Chitta L P, Syntelis P *Astrophys. J. Lett.* **862** L24 (2018)
98. Syntelis P, Priest E R, Chitta L P *Astrophys. J.* **872** 32 (2019)
99. Syntelis P, Priest E R *Astrophys. J.* **891** 52 (2020)
100. Smitha H N et al. *Astrophys. J. Suppl.* **229** 17 (2017)
101. Tiwari S K et al. *Astrophys. J. Lett.* **795** L24 (2014)
102. Ellerman F *Astrophys. J.* **46** 298 (1917)
103. Pariat E et al. *Astron. Astrophys.* **473** 279 (2007)
104. Watanabe H et al. *Astrophys. J.* **736** 71 (2011)
105. Hong J et al. *Astrophys. J.* **792** 13 (2014)
106. Kitai R *Solar Phys.* **87** 135 (1983)
107. Fang C et al. *Astrophys. J.* **643** 1325 (2006)
108. Rezaei R, Beck C *Astron. Astrophys.* **582** A104 (2015)
109. Reid A et al. *Astrophys. J.* **823** 110 (2016)
110. Georgoulis M K et al. *Astrophys. J.* **575** 506 (2002)
111. Vissers G J M et al. *Astrophys. J.* **774** 32 (2013)
112. Peter H et al. *Science* **346** 1255726 (2014)
113. Kim Y-H et al. *Astrophys. J.* **810** 38 (2015)
114. Libbrecht T et al. *Astron. Astrophys.* **598** A33 (2017)
115. Rutten R J et al. *J. Phys. Conf. Ser.* **440** 012007 (2013)
116. Vissers G J M et al. *Astrophys. J.* **812** 11 (2015)
117. Hansteen V H et al. *Astrophys. J.* **839** 22 (2017)
118. Reid A et al. *Astrophys. J. Lett.* **835** L37 (2017)
119. Schmieder B et al. *Astrophys. J.* **601** 530 (2004)
120. Bello González N, Danilovic S, Kneer F *Astron. Astrophys.* **557** A102 (2013)
121. Pariat E et al. *Astrophys. J.* **614** 1099 (2004)
122. Pariat E et al. *Adv. Space Res.* **38** 902 (2006)
123. Nelson C J et al. *Astrophys. J.* **779** 125 (2013)
124. Nelson C J et al. *Astrophys. J.* **798** 19 (2015)
125. Diver D A, Brown J C, Rust D M *Solar Phys.* **168** 105 (1996)
126. Danilovic S *Astron. Astrophys.* **601** A122 (2017)
127. Parker E N *Astrophys. J.* **145** 811 (1966)
128. Magara T *Astrophys. J.* **549** 608 (2001)
129. Isobe H, Tripathi D, Archontis V *Astrophys. J. Lett.* **657** L53 (2007)
130. Archontis V, Hood A W *Astron. Astrophys.* **508** 1469 (2009)
131. Litvinenko Yu E *Astrophys. J.* **515** 435 (1999)
132. Madjarska M S *Living Rev. Sol. Phys.* **16** 2 (2019)
133. Vaiana G S et al. *Astrophys. J.* **185** L47 (1973)
134. Kankelborg C C et al. *Astrophys. J.* **466** 529 (1996)
135. Brown D S et al. *Solar Phys.* **201** 305 (2001)
136. Chandrashekhar K et al. *Solar Phys.* **286** 125 (2013)
137. Habbal S R et al. *Astrophys. J.* **306** 740 (1986)
138. Fu Q, Kundu M R, Schmahl E J *Solar Phys.* **108** 99 (1987)
139. Habbal S R, Harvey K L *Astrophys. J.* **326** 988 (1988)
140. Nitta N et al. *Publ. Astron. Soc. Jpn.* **44** L167 (1992)
141. Habbal S R, Dowdy J F (Jr.), Withbroe G L *Astrophys. J.* **352** 333 (1990)
142. Zhang J, Kundu M R, White S M *Solar Phys.* **198** 347 (2001)
143. Alipour N, Safari H *Astrophys. J.* **807** 175 (2015)
144. Sheeley N R (Jr.), Golub L *Solar Phys.* **63** 119 (1979)
145. Kotoku J et al. *Publ. Astron. Soc. Jpn.* **59** S735 (2007)
146. Pérez-Suárez D et al. *Astrophys.* **492** 575 (2008)
147. Mou C et al. *Astrophys. J.* **818** 9 (2016)
148. Golub L, Krieger A S, Vaiana G S *Solar Phys.* **49** 79 (1976)
149. Hirzberger J et al. *Solar Phys.* **251** 417 (2008)
150. Alexander C E, Del Zanna G, Maclean R C *Astron. Astrophys.* **526** A134 (2011)
151. Kariyappa R et al. *Astron. Astrophys.* **526** A78 (2011)
152. Habbal S R, Grace E *Astrophys. J.* **382** 667 (1991)
153. Brosius J W et al. *Astrophys. J.* **677** 781 (2008)
154. Doschek G A et al. *Astrophys. J.* **710** 1806 (2010)
155. Nolte J T, Solodyna C V, Gerassimenko M *Solar Phys.* **63** 113 (1979)
156. Preś P, Phillips K H J *Astrophys. J.* **510** L73 (1999)
157. Madjarska M S et al. *Astron. Astrophys.* **398** 775 (2003)
158. Ugarte-Urra I et al. *Astron. Astrophys.* **418** 313 (2004)
159. Tian H, Xia L-D, Li S *Astron. Astrophys.* **489** 741 (2008)
160. Habbal S R, Withbroe G L *Solar Phys.* **69** 77 (1981)
161. Strong K T et al. *Publ. Astron. Soc. Jpn.* **44** L161 (1992)
162. Kayshap P, Dwivedi B N *Solar Phys.* **292** 108 (2017)
163. Zhang P, Fang C, Zhang Q *Sci. China Phys. Mech. Astron.* **55** 907 (2012)
164. Kankelborg C C, Walker A B C (II), Hoover R B *Astrophys. J.* **491** 952 (1997)
165. Mandrini C H et al. *Solar Phys.* **168** 115 (1996)
166. Krieger A S, Vaiana G S, van Speybroeck L P, in *Solar Magnetic Fields* (IAU Symp., Vol. 43, Ed. R Howard) (Dordrecht: Springer, 1971) p. 397
167. Vaiana G S, Krieger A S, Timothy A F *Solar Phys.* **32** 81 (1973)
168. Tang F et al. *Adv. Space Res.* **2** (11) 65 (1982)
169. Harvey K L et al., in *Solar Active Region Evolution: Comparing Models with Observations. Proc. of the 14th Intern. Summer Workshop, Sunspot, New Mexico, USA, 30 August–3 September 1993* (Astronomical Society of the Pacific Conf. Ser., Vol. 68, Eds K S Balasubramaniam, G W Simon) (San Francisco, CA: Astronomical Society of the Pacific, 1994) p. 377
170. Galsgaard K et al. *Astron. Astrophys.* **606** A46 (2017)
171. Longcope D W et al. *Astrophys. J.* **553** 429 (2001)
172. Harvey K L et al. *Adv. Space Res.* **13** (9) 27 (1993)
173. Webb D F et al. *Solar Phys.* **144** 15 (1993)
174. Parnell C E, Priest E R, Titov V S *Solar Phys.* **153** 217 (1994)
175. Parnell C E, Priest E R, Golub L *Solar Phys.* **151** 57 (1994)
176. Priest E R, Parnell S E, Martin S F *Astrophys. J.* **427** 459 (1994)
177. Van Driel-Gesztelyi L et al. *Solar Phys.* **163** 145 (1996)
178. Kontogiannis I et al. *Astron. Astrophys.* **633** A67 (2020)
179. Longcope D W *Astrophys. J.* **507** 433 (1998)
180. McIntosh S W *Astrophys. J.* **670** 1401 (2007)
181. Hui T et al. *Astrophys. J.* **681** L121 (2008)
182. Ulyanov A S et al. *Solar Phys.* **294** 128 (2019)
183. Bogachev S A et al. *Astrophys. J.* **630** 561 (2005)
184. Craig I J D, Sneyd A D *Astrophys. J.* **311** 451 (1986)
185. Golub L et al. *Solar Phys.* **243** 63 (2007)
186. Reale F et al. *Astrophys. J. Lett.* **736** L16 (2011)
187. Warren H P, Winebarger A R, Brooks D H *Astrophys. J.* **759** 141 (2012)
188. Testa P, Reale F *Astrophys. J. Lett.* **750** L10 (2012)
189. Reale F et al. *Astrophys. J.* **698** 756 (2009)
190. Schmelz J T et al. *Astrophys. J.* **704** 863 (2009)
191. Schmelz J T et al. *Astrophys. J.* **693** L131 (2009)
192. Testa P et al. *Astrophys. J.* **728** 30 (2011)
193. Winebarger A R et al. *Astrophys. J. Lett.* **746** L17 (2012)
194. Hannah I G et al. *Astrophys. J. Lett.* **820** L14 (2016)
195. Harrison F A et al. *Astrophys. J.* **770** 103 (2013)
196. Ishikawa S et al. *Publ. Astron. Soc. Jpn.* **66** S15 (2014)
197. Krucker S et al. *Astrophys. J. Lett.* **793** L32 (2014)
198. Del Zanna G, Mason H E *Astron. Astrophys.* **565** A14 (2014)
199. Miceli M et al. *Astron. Astrophys.* **544** A139 (2012)
200. Gburek S et al. *Solar Syst. Res.* **45** 189 (2011); *Astron. Vestn.* **45** 195 (2011)
201. Sylwester B, Sylwester J, Phillips K J H *Astron. Astrophys.* **514** A82 (2010)
202. Sylwester J et al. *Solar Phys.* **226** 45 (2005)
203. Reva A et al. *Solar Phys.* **293** 140 (2018)
204. Parenti S et al. *Astrophys. J.* **846** 25 (2017)
205. Wilhelm K et al. *Solar Phys.* **162** 189 (1995)
206. Brosius J W, Daw A N, Rabin D M *Astrophys. J.* **790** 112 (2014)
207. Oraevsky V N, Sobelman I I *Astron. Lett.* **28** 401 (2002); *Pis'ma Astron. Zh.* **28** 457 (2002)
208. Cargill P J *Astrophys. J.* **784** 49 (2014)
209. Kuznetsov V D et al. *Geomagn. Aeron.* **56** 781 (2016)
210. Kuzin S V et al. *Bull. Russ. Acad. Sci. Phys.* **75** 87 (2011); *Izv. Ross. Akad. Nauk Fiz.* **75** 91 (2011)
211. Vishnyakov E A et al. *Proc. SPIE* **10235** 102350B (2017)